NATURAL RESOURCES

GEOLOGIC MAP OF THE LITTLEROCK 7.5-MINUTE QUADRANGLE, THURSTON COUNTY, WASHINGTON

by Michael Polenz, Jessica L. Vermeer, Gabriel Legorreta Paulín, Jeffrey H. Tepper, Shannon A. Mahan, and Recep Cakir

WASHINGTON
GEOLOGICAL SURVEY
Map Series 2017-01
October 2017

INTERNALLY REVIEWED

WASHINGTON STATE DEPARTMENT OF
NATURAL RESOURCES
WASHINGTON GEOLOGICAL SURVEY

GEOLOGIC MAP OF THE LITTLEROCK 7.5-MINUTE QUADRANGLE, THURSTON COUNTY, WASHINGTON

by Michael Polenz, Jessica L. Vermeer, Gabriel Legorreta Paulín, Jeffrey H. Tepper, Shannon A. Mahan, and Recep Cakir

WASHINGTON
GEOLOGICAL SURVEY
Map Series 2017-01
October 2017

This geologic map was funded in part by the USGS National Cooperative Geologic Mapping Program, award no. G16AC00286

This publication has been subject to an iterative technical review process by at least one Survey geologist who is not an author. This publication has also been subject to an iterative review process with Survey editors and cartographers.

WASHINGTON STATE DEPARTMENT OF
NATURAL RESOURCES
WASHINGTON GEOLOGICAL SURVEY

DISCLAIMER

Neither the State of Washington, nor any agency thereof, nor any of their employees, makes any warranty, express or implied, or assumes any legal liability or responsibility for the accuracy, completeness, or usefulness of any information, apparatus, product, or process disclosed, or represents that its use would not infringe privately owned rights. Reference herein to any specific commercial product, process, or service by trade name, trademark, manufacturer, or otherwise, does not necessarily constitute or imply its endorsement, recommendation, or favoring by the State of Washington or any agency thereof. The views and opinions of authors expressed herein do not necessarily state or reflect those of the State of Washington or any agency thereof.

INDEMNIFICATION

Research supported by the U.S. Geological Survey, National Cooperative Geologic Mapping Program, under USGS award number G16AC00286. The views and conclusions contained in this document are those of the authors and should not be interpreted as necessarily representing the official policies, either expressed or implied, of the U.S. Government.

WASHINGTON STATE DEPARTMENT OF NATURAL RESOURCES

Hilary S. Franz—*Commissioner of Public Lands*

WASHINGTON GEOLOGICAL SURVEY

David K. Norman—*State Geologist*
Timothy J. Walsh—*Assistant State Geologist*
John P. Bromley—*Assistant State Geologist*

Washington State Department of Natural Resources
Washington Geological Survey

Mailing Address:
MS 47007
Olympia, WA 98504-7007

Street Address:
Natural Resources Bldg, Rm 148
1111 Washington St SE
Olympia, WA 98501

Phone: 360-902-1450
Fax: 360-902-1785
Email: geology@dnr.wa.gov
Website: http://www.dnr.wa.gov/geology

Publications and Maps:
www.dnr.wa.gov/programs-and-services/geology/publications-and-data/publications-and-maps

Washington Geology Library Searchable Catalog:
www.dnr.wa.gov/programs-and-services/geology/washington-geology-library

Suggested Citation: Polenz, Michael; Vermeer, J. L.; Legorreta Paulín, Gabriel; Tepper, J. H.; Mahan, S. A.; Cakir, Recep, 2017, Geologic map of the Littlerock 7.5-minute quadrangle, Thurston County, Washington: Washington Geological Survey Map Series 2017-01, 1 sheet, scale 1:24,000, 36 p. text. [http://www.dnr.wa.gov/publications/ger_ms2017-01_geol_map_littlerock_24k.zip]

Contents

FIGURES

TABLES

MAP SHEET

Geologic Map of the Littlerock 7.5-minute Quadrangle, Thurston County, Washington

by Michael Polenz[1], Jessica L. Vermeer[1], Gabriel Legorreta Paulín[2], Jeffrey H. Tepper[3], Shannon A. Mahan[4], and Recep Cakir[1]

[1] Washington Geological Survey
MS 47007
Olympia, WA 98504-7007

[2] Instituto de Geografía
Universidad Nacional Autónoma de México
Ciudad Universitaria, Del Coyoacán
cp 04510, México, D.F.

[3] Geology Department
University of Puget Sound
1500 N Warner
Tacoma, WA 98416 U.S.

[4] Geological Survey
Box 25046, MS 974
Denver Federal Center
Denver, CO 80225-5046

INTRODUCTION

The Littlerock 7.5-minute quadrangle in Thurston County, Washington, straddles the east side of the Black Hills and the Black River valley in the southwestern Puget Lowland. It includes the town of Littlerock 14 mi south of Olympia. Much of the quadrangle is within Capitol State Forest, a popular recreation area and active timber resource managed by Washington State. The hillslopes are prone to hazardous and destructive landslides, earthflows, and debris flows, especially where soils are thick and clayey. The lowlands are agriculturally important and ecologically sensitive, with extensive wetlands, large tracts of the Black River Unit of the Billy Frank Jr. Nisqually National Wildlife Refuge along the Black River valley, and enigmatic soil mounds in the Mima Mounds Natural Area and elsewhere on glacial outwash terraces. Groundwater flooding is a known hazard in parts of the lowlands, and the need to manage water for drinking and irrigation is increasing. The detailed mapping completed in this study will help identify these hazards and inform public and private resource management.

GEOLOGIC OVERVIEW

Bedrock

Most of the Littlerock quadrangle is underlain by early to middle Eocene basalt of the upper Crescent Formation (Noble and Wallace, 1966; Globerman, 1981; Globerman and others, 1982; Logan, 1987; Walsh and others, 1987). The Crescent Formation is part of the Siletzia terrane, a large igneous province composed of submarine to subaerial tholeiitic and alkalic basalt extruded near the margin of North America between 56 and 48.4 Ma (Glassley, 1974; Irving, 1979; Babcock and others, 1992, 1994; Wells and others, 2014; Eddy and others, 2017). Siletzia was accreted to North America at approximately 50 Ma (Trehu and others, 1994; Wells and others, 2014; Eddy and others, 2017) and is exposed in the eastern Black Hills throughout the west half of the quadrangle. Farther east, bedrock is mostly concealed beneath Quaternary glacial sediment, but isolated exposures of basaltic rock (Walsh and others, 1987; Schasse, 1987; Walsh and Logan, 2005; Logan and others, 2009) and gravity and aeromagnetic data suggest that basaltic bedrock continues in the subsurface. This inference is also consistent with seismic imaging (Trehu and others, 1994; Parsons and others, 1999; Schmandt and Humphreys, 2011) and tomographic modeling (Gao and others, 2011), both of which suggest that a subsurface slab of basalt extends farther east. Within the Black Hills, basalt has been argon-dated at ~55 to 50 Ma (Duncan, 1982; Globerman and others, 1982; Czajkowski, 2016; Polenz and others, 2016). U-Pb ages suggest that Siletzia at the latitude of Washington State ranges in age from 53.2 to 48.4 Ma (Eddy and others, 2017).

Northeast, east, and southeast of the Littlerock quadrangle, Eocene and younger volcanic and mostly Cascade Range–derived sedimentary rocks post-date the Crescent Formation (Snavely and others, 1951, 1958; Dragovich and others, 2002; Walsh and Logan, 2005; Logan and others, 2009; Kant and others, 2015). Tertiary marine and terrestrial sediments onlap the Crescent Formation on the southern and western flanks of the Black Hills (Pease and Hoover, 1957; Snavely and others, 1958; Noble and Wallace, 1966; Logan, 1987, 2003; Walsh and others, 1987) and probably also in the subsurface along the eastern flank. Of these onlapping Tertiary sedimentary rocks, only the middle Eocene McIntosh Formation has been recognized in the Littlerock quadrangle, where it appears to overlie Crescent Formation at the southeast margin of the Black Hills (Snavely and others, 1958; Noble and Wallace, 1966). This onlapping relation and tectonic reconstructions (Wells and others, 2014; Eddy and others, 2017) suggest that the Black Hills were at least partly uplifted during the Eocene (Pratt and others, 1997). Folding and faulting of the Tertiary sedimentary rocks also point to more recent deformation (Snavely and others, 1958; Logan, 1987; Schasse, 1987; Walsh and others, 1987).

Surficial Deposits

The Black River valley occupies the east half of the Littlerock quadrangle along the western margin of the southern Puget Lowland. The lowland was repeatedly overridden by the Puget lobe of the Cordilleran continental ice sheet, resulting in a locally thick, stratigraphically complex cover of Quaternary sediments. The most recent Cordilleran ice incursion was the Vashon stade

of the Fraser glaciation (MIS 2[1]), which covered the east half of the map area and extended a few miles south of it. Vashon and older till and outwash and postglacial Black River valley sediment (Noble and Wallace, 1966; Logan, 1987; Walsh and others, 1987) conceal the contact and any structures between the Crescent Formation in the Black Hills and Tertiary volcanic and sedimentary bedrock east of the Black River (Snavely and others, 1958; Noble and Wallace, 1966; Lea, 1984; Logan, 1987; Schasse, 1987; Walsh and others, 1987; Walsh and Logan, 2005; Logan and others, 2009).

Tectonic Framework

The Littlerock quadrangle is within the forearc of the Cascadia subduction zone, where oblique subduction of the Juan de Fuca plate beneath the North American plate has resulted in structural complexity (Wells and others, 1998; Lewis and others, 2003; Johnson and others, 2004; McCaffrey and others, 2007, 2013). Ongoing northwest translation of the Sierra Nevada block causes clockwise rotation of the Oregon forearc (Wells and McCaffrey, 2013) and clockwise rotation of discrete crustal blocks within the Washington forearc (Wells and others, 1998). Wells and others (2017) suggested that steeply dipping faults bound these blocks. In the Black Hills, this rotation is about 29° clockwise in reversely and normally magnetized Eocene basalt (Globerman, 1981; Globerman and others, 1982). Globerman (1981) added that the Black Hills are a 10 to 15° west-dipping homocline wherein units are not appreciably folded but are commonly cut by normal and reverse faults.

The clockwise rotation of the Washington forearc is accompanied by north–south shortening against the relatively stable Coast Mountains of British Columbia. This shortening has resulted in a series of basins and uplifts bounded by mostly east–west-trending reverse faults and folds (Clowes and others, 1987; Johnson and others, 1996; Wang, 1996; Pratt and others, 1997; Wells and others, 2017; Bowman and Czajkowski, 2016). Some tectonic models of the Washington forearc, such as that proposed by Pratt and others (1997), require ongoing crustal shortening south of Olympia. This suggests that some structures south and southwest of Olympia (Fig. M1) are active. Wells and others (2017) theorize that spatially ordered distribution of subduction-related, ongoing episodic tremor and slip events suggests kinematic linkage of crustal faults to active Cascadia subduction, thus also suggesting active crustal faulting in the area.

[1] MIS: global *m*arine oxygen *i*sotope *s*tage curve, where even-numbered stages are used as proxy for timing and intensity of global glacial periods (Morrison, 1991). For discussion of corresponding Cordilleran ice sheet advances into the Puget Lowland, see Booth and others (2004), Troost and Booth (2008), Polenz and others (2013, 2015), and Troost (2016). For timing of the MIS 2 ice advance into the map area at the southern limit of the Vashon glaciation, we refer to Polenz and others' (2015) figure 3 and discussion, although the southern tip of their figure 3 should have been extended south of Olympia to the latitude of the Littlerock quadrangle.

METHODS

Geologic Mapping

We identified units from field observations between July 1 and October 31, 2016, supplemented by short field visits between November 2016 and February 2017. We used thin-section analyses, well and boring records, geotechnical reports, geophysical data, prior geologic mapping, geomorphic features identified from lidar, soil maps by the U.S. Department of Agriculture (USDA, 2013), and aerial orthophotos to refine the mapping. We reviewed 1,332 water wells and geotechnical borings (Jeschke and others, 2016; WGS internal records) in and within ~1 mi of the Littlerock quadrangle; we could precisely locate 600 and used those to inform our mapping. Locations of 22 wells are shown on the map; these are wells that we identified as best-located and most geologically informative inside the quadrangle. For 138 wells, we transcribed driller's log information and assigned depth intervals to apparent lithology and likely geologic unit. We used lidar-based elevation data with 2-m-grid resolution to derive hillshade images, contours, and other products. We adapted methods outlined by Singhroy and others (1992a,b) for LANDSAT satellite image analysis, calibrated by our field observations, to identify surface sediment particle sizes and bedrock character in order to refine our unit boundaries. Edge mismatches with the adjacent Summit Lake and Maytown quadrangles are intentional and based on differences in unit classifications or interpretation. We used the geologic time scale of the USGS Geologic Names Committee (2010); where that scale lacked Epoch subdivisions, we referred to Walker and Geissman (2009). We used the Udden-Wentworth scale (table 5 in Pettijohn, 1957) to classify unconsolidated sediment.

Measurements of Structural Features

We collected strike and dip measurements of joints and shears in bedrock where outcrops suggested more than random cracks, brecciation of unknown origin, or columnar joints in basalt. Most outcrops were small, and no measured features could be traced beyond individual outcrops.

Terrain Analysis (Lineaments and Streams))

We analyzed topographic lineaments throughout the Black Hills and beyond. We excluded lineaments that we interpreted as expressions of ice flow, such as drumlins. Lineament identification was conducted systematically at several scales using lidar-derived digital elevation model (DEM) hillshades, and slope and aspect models. Straight stream reaches were included in the analysis by first creating a stream network using ArcGIS hydrology tools, then using the linear directional mean tool to find the average flow direction for stream reaches.

Geophysical Data and Analysis

Passive and active seismic data were collected by WGS in support of this mapping project to provide depth-to-bedrock estimates for selected locations where well records failed to penetrate bedrock and aeromagnetic data suggested bedrock surface contrasts with possible structural implications, or where other considerations caught our interest. Methods included:

- Single station, passive seismic Horizontal-to-Vertical Spectral Ratio analysis (HVSR) using a Tromino ZERO® three-component seismograph (operating range 0.1–64 Hz; http://tromino.eu/prodsel.asp?cat=1&prod=1).
- Multi-sensor, single-channel (4.5 Hz) passive seismic survey using Microtremor Array Measurements (MAM).
- Multichannel Analysis of Surface Waves (MASW) active seismic survey using 4.5 Hz geophones and a 16 lb sledge hammer.
- Ground-Penetrating Radar (GPR) survey to image sediment above shallow-basalt.
- MAM, MASW, and GPR analyses to calibrate analysis of HVSR data.

Tentative interpretations for selected sites that yielded insightful, high-quality data are shown on the map as geophysical data collection localities.

STRUCTURAL ANALYSIS

Topographic lineaments and structural measurements were compared to max spot clusters[2], other anomalies, and lineaments in several aeromagnetic images generated by Richard Blakely (USGS, written commun., 2016). Orientations were evaluated using stereonet software and Microsoft Excel®. Gravity data were considered but mostly proved too coarse to add insight. All of these data were evaluated in the context of known structures near the map area.

Geochronology and Paleontology

Table M1 summarizes results from: (1) one new radiocarbon date on wood, (2) new optically stimulated and infrared-stimulated luminescence analyses on one sample of sand, (3) a new $^{40}Ar/^{39}Ar$ date on basalt, (4) a new U-Pb date by laser-ablation ICP-MS on zircon, and (5) foraminiferal biostratigraphic (paleontological) analyses from seven new sedimentary bedrock samples within the Littlerock quadrangle and nine new samples collected for reference from known units outside the map area. Details about the samples and analyses are presented in Appendices A to D (except for biostratigraphic samples) and the Data Supplement (DS). Biostratigraphy samples were prepared by Ellington and Associates, Inc. (Houston, TX, division of ALS) for microfossil analysis, and fossil content was analyzed by Elizabeth Nesbitt (Burke Museum, Univ. of Wash.).

Geochemistry

BEDROCK, DRIFT, AND CLAY

Major and trace element analyses were performed on 51 samples; of basalt, sedimentary rocks, drift, and weathering products of bedrock and drift. Major and trace element analysis were performed by ALS (geochemistry laboratory in North Vancouver, BC, Canada)(Tables DS7 and DS8 in the Data Supplement identify the method for each analyte). We used geochemical plots to compare our new igneous bedrock samples to compilations of other igneous rocks in western Washington. We compared the geochemical characteristics of sedimentary rock samples within the map area to samples we collected where Snavely and others (1958) had mapped Eocene to Miocene units outside the Littlerock quadrangle.

Analyses of clay-rich soils and saprolites are presented in Tables DS7 and DS8. Additional x-ray diffraction (XRD) clay-mineral identification on selected samples (three from sedimentary bedrock, five apparently from drift, and seven apparently from basalt) are presented in Tables DS9 and DS10 (analyses by Sietronics Laboratory Services, Mitchell ACT 2911, Australia).

PLACER GOLD

Alluvial sediment from selected streams was tested to assess the gold production potential of streams in the map area and their source rocks. To assess Black Hills–derived sediment unaffected by ice incursions, we included one sample site west of the map area. We collected samples from active channels on five streams and separately analyzed splits as (1) bulk sample and (2) panned sample. Both sample types were dry sieved and only the –35 sieve size fraction (selecting for analysis all particles 0.5 mm or smaller in diameter) was included in the geochemical analysis. Geochemistry included gold extraction by fire assay, as well as analyses for 35 other elements by inductively coupled plasma atomic emission spectroscopy (ICP-AES; Table DS11), and was performed by ALS.

Sedimentary Provenance of Quaternary Units

We used clast counts (Table DS5), petrographic review of matrix content (Table DS6), sedimentary attributes (such as bedding style, grain size, and textural changes), and field relations among unlithified deposits to infer provenance of sedimentary units and help determine their depositional setting (glacial, nonglacial, or undivided).

For clast counts in unconsolidated Quaternary-aged units, we recorded pebble clast lithology and weathering to determine provenance and help assess relative deposit ages. Northern-sourced clast assemblages were defined based on the clast content of Vashon Till and outwash, which are readily apparent as the most recent glacial sediments in the Littlerock quadrangle. Outwash deposits with known, partly Cascades-sourced origin in unit Qgo$_{y3}$ were used to define clast assemblages that suggest Cascades provenance. Black Hills provenance was defined by modern alluvium in Black Hills drainages west of the Vashon and pre-Vashon ice limits.

Quaternary Geochronology

WEATHERING

The relative ages of Quaternary units were assessed using clast weathering and thin-section petrographic assessment of matrix

[2] Locations of anomalously large aeromagnetic field strength gradients, objectively identified by curvature analysis, which assumes that contacts are vertical and remanent magnetization is unimportant (Richard Blakely, USGS, written commun., 2013). See Blakely and others (2004) for a description of aeromagnetic max-spots methodology.

weathering. The results are tabulated in the Data Supplement (Tables DS5 and DS6) and discussed below (see *Weathering*).

RADIOCARBON ANALYSIS

Conventional radiocarbon analysis was performed on wood from a fine-grained bed in unit Qoa. The sample was zip-lock bagged on-site (air tight and saturated) and oven-dried at the WGS lab a few days later. Conventional "radiocarbon plus" analysis was performed by Beta Analytic (Miami, FL).

LUMINESCENCE AGE ANALYSIS

Luminescence dating was performed on a Qpo_2 fluvial deposit along Waddell Creek. One sand sample was collected by pounding an opaque metal tube into a sand exposure. To minimize light exposure, we sampled a shady location on an overcast to rainy late afternoon and shielded the exposure with a dark cloth while surficial sand was removed and the sample tube was inserted, removed, and sealed in the sample tube. Optically stimulated (quartz) and infrared-stimulated (feldspar) luminescence analyses were performed by Shannon Mahan and Harrison Gray (USGS, Denver, CO).

DESCRIPTION OF MAP UNITS

Quaternary Unconsolidated Deposits

POSTGLACIAL DEPOSITS

Postglacial deposits in glaciated parts of the map area are in most cases readily identified by their lack of compaction. However, there are exceptions, and in unglaciated parts of the map area, glacial/postglacial distinctions are difficult and commonly meaningless. These issues are further discussed below (see *Nonglacial Deposits* discussion below).

Holocene Nonglacial Deposits

ml **Modified land**—Basalt and basaltic rubble or northern-sourced cobbles, pebbles, sand, and boulders in varied amounts; locally derived but redistributed to modify topography; underlying units exposed in some areas; shown in four rock quarries where redistribution of material appears likely to mask underlying deposits; excludes roads and some pits where underlying units can be readily identified, fill areas appear minor, excavation exposes the same unit as the surrounding surface, or exposure of underlying units was deemed likely to be permanent.

Qp **Peat**—Organic and organic-rich sediment; includes peat, gyttja, muck, silt, and clay; typically in closed depressions; Rigg (1958) recorded as much as 30 ft of peat in the Black River valley; mapped in wetland areas and distinctly flat-bottomed depressions; also mapped on the basis of spectral analysis of LANDSAT data and (or) evaluation of infrared and color aerial photos.

Qls **Landslide deposits**—Cobbles, pebbles, sand, silt, clay, boulders, and diamicton of basalt, siltstone, and sandstone in varied amounts within areas of mass-wasting; weathering varied; clasts angular to rounded; unsorted; generally loose, jumbled, and unstratified, but locally retaining primary bedding and compaction; rock types varied but basalt-rich; derived from units upslope (or underfoot in some landslide toes). Some slide areas include exposures of underlying units. Unit thickness varies throughout the map area and is mostly unassessed. Some deposits exceed 20 ft in part of a historically active landslide in the SW¼ NW¼ sec. 33, T17N R3W. Landslides were mapped only where their deposits could be confidently identified and are extensive enough to show at map scale. Our mapping of landslides was informed in part by reconnaissance landslide mapping carried out by WGS landslide geologists in preparation for our mapping (Trevor Contreras, WGS, written commun., 2016). Valley-floor runout deposits from debris flows and associated floods are included with unit Qa. Landforms that suggest landslides abound in the map area, especially south and west of the Vashon ice limit. In most instances, the extent of these landforms is morphologically vague, and other attributes commonly associated with slope movement, such as stressed vegetation or disrupted drainage, are absent or ambiguous. Such landforms cover a large part of the map area but the presence of landslide deposits is uncertain. They are identified by the 'Mass Wasting' feature overlay pattern (see *Geologic Symbols* on plate). Many landslides are unmapped because steep slopes or streams have dispersed their deposits. Those concerned with slope stability are additionally referred to the WGS landslide inventory (WGS, 2016a) and topical studies, such as Sarikhan and others (2008, 2009). Absence of a mapped slide does not imply stability or absence of hazard.

Pleistocene to Holocene Nonglacial Deposits

Qa, Qoa **Alluvium**—Pebbles, cobbles, sand, silt, clay, peat, and boulders in varied amounts along stream channels and on flood plains; mapped as unit Qoa where active channels no longer contribute to the deposit; clasts and matrix generally gray or olive gray, or dark brown due to organic matter, locally iron-stained red or yellowish brown; fresh or lightly weathered east of Vashon ice limit, except where deposits include material proximally reworked from older deposits, locally resulting in a bimodal clast weathering pattern such as at clast count site C45 (sec. 21, T17N R3W); fresh to heavily weathered (all clay) in unglaciated and pre-Vashon glaciated areas, where clay weathering is commonly inherited from soils washed in from upslope (Bretz, 1913). Subunit Qoa is pale tannish gray, red, or weathered to yellowish or orange-brown; loose; clasts typically well rounded and moderately to well sorted; matrix cementation light or absent, even where deposits are matrix-supported; thinly bedded to massive; derived from local sources and deposited in streams and on flood plains.

Alluvium from the Black Hills can consist entirely of basalt, as illustrated by clast count C6 (sec. 12, T16N R4W), but where watersheds include glacial deposits,

the alluvium will include northern-sourced clasts, as illustrated by clast counts at sites C44 (Schematic Section 1, sec. 34, T17N R3W), C45 (sec. 21, T17N R3W), and C38 (unit Qoa, sec. 17, T16N R3W). Where units Qa and Qoa incorporate northern-sourced lithologies, they tend to resemble unit Qgo and are distinguished from Qgo by field relations and, usually, less sorting than in unit Qgo. Many deposits of units Qa and Qoa also contain more matrix sand and (or) mud than unit Qgo. Unit Qa includes locally voluminous deposits from debris flows and associated floods, such as at the confluences of Petosi Creek and Camp Four Creek into Waddell Creek (sec. 5, T17N R3W), where bouldery debris-flow runout deposits from December 2007 (Sarikhan and others, 2008) exceed 10 ft in thickness, and a decade after the event, trimlines among nearby trees still bear witness to flood heights more than 10 ft above the post-event flood plain. Depositional age for unit Qa is mostly Holocene but, at least for subunit Qoa, ranges to Vashon or pre-Vashon age, as illustrated by age site GD1 (see *Nonglacial Deposits* and Tables M1 and A1).

Qaf **Alluvial fan deposits**—Pebbles, sand, silt, clay, cobbles, and boulders in varied amounts; gray to brown; fresh to lightly weathered east of Vashon ice limit; fresh to heavily weathered (all clay) in pre-Vashon glaciated and unglaciated areas; loose; clasts subangular to rounded; moderately to poorly sorted; stratified to poorly stratified; derived from local sources, but those local sources commonly include material reworked from distant (northern or Cascade Range) sources; deposited in concentric lobes where streams emerge from confining valleys. Morphology in most cases suggests 10 to 20 ft maximum thickness. Deposition at the base of hillslopes is commonly sudden, hazardous, and associated with significant storm events. In many deposits, much or most of the fan volume is of (late) Vashon age because geomorphic processes then were more active than throughout postglacial time (Ballantyne, 2002).

PLEISTOCENE GLACIAL DEPOSITS

Vashon Drift of the Fraser Glaciation

Qgo **Recessional Vashon outwash, undivided**—Pebbles, cobbles, sand, and silt in varied amounts; light gray where fresh, weathering to pale brown or tan, light orange where iron stained; lightly weathered, with most weathering rinds less than 2 mm thick; loose; well sorted; clasts well rounded; massive to bedded; may locally be lightly cemented; clast lithologies are northern-sourced (Fig. 1) with ~50–70% basalt, ~10% each of granitic and intermediate igneous rocks, and lesser amounts of high-grade metamorphic and other rocks. Unit Qgo thickness is likely no more than a few feet in erosional outwash channels. Maximum observed thickness is 60 ft beneath a relict terrace (inselberg) east of Waddell Creek (sec. 21, T17N R3W), and well records suggest more than 120 ft near the southern map boundary.

Vashon recessional outwash was deposited by meltwater from the Cordilleran ice sheet. Unit Qgo is stratigraphically above units Qga, Qgt, and Qgic, but its largest deposits form broad, relict terraces in erosional troughs flanked by these units. The unit includes kame deposits along the eastern flank of the Black Hills. Some areas of Vashon recessional terraces are topped by Mima Mounds, indicated by the Mima Mounds feature overlay pattern where landforms and (or) field-observed deposits indicate their presence. Their physical characteristics and enigmatic origin are discussed in *Ages of Deposits and Paleoenvironmental Interpretation*. Unit Qgo is distinguished from similar postglacial alluvium by field relations that signal deposition by meltwater from Vashon ice. Some deposits were assigned to the unit on the rationale that periglacial erosion and sedimentation was more vigorous than ongoing processes (Ballantyne, 2002), and postglacial conditions appear to lack the fluvial vigor required to assemble the observed deposits. Divided into:

Qgoaf **Vashon recessional alluvial fan deposits**—Pebbles, sand, silt, clay, cobbles, and boulders in varied amounts; gray to brown; fresh to lightly weathered east of Vashon ice limit, more clay-rich and therefore more weathered west of Vashon ice limit; loose; clasts subangular to rounded; moderately to poorly sorted; stratified to poorly stratified; derived from local sources, but includes material reworked from distant (northern or Cascade Range) sources; deposited in concentric lobes where streams emerge from confining valleys. Morphology suggests 10 to 20 ft maximum thickness. Unit Qgoaf forms relict fan deposits dissected by modern streams that no longer appear to flood onto or migrate across the fan surface. We infer a late-Vashon depositional age because geomorphic processes then were more active than throughout postglacial time (Ballantyne, 2002).

Qgog **Vashon recessional outwash gravel**—Pebble to cobble gravel with a coarse sand matrix; gray or tan, red-orange where iron stained; lightly weathered, with most weathering rinds less than 2 mm thick; loose; may be lightly cemented; clasts are subrounded to well rounded and well sorted; massive to bedded with localized interbeds or lenses of sand, with little to no silt or clay; clast lithologies are northern-sourced (Fig. 1) with ~50–70% basalt, ~10% each of granitic and intermediate igneous rocks, and lesser amounts of high-grade metamorphic and other rocks. Thickness is difficult to constrain in all areas, but 25 ft was observed at the DNR gravel pit on Mima Prairie (sec. 10, T16N R3W).

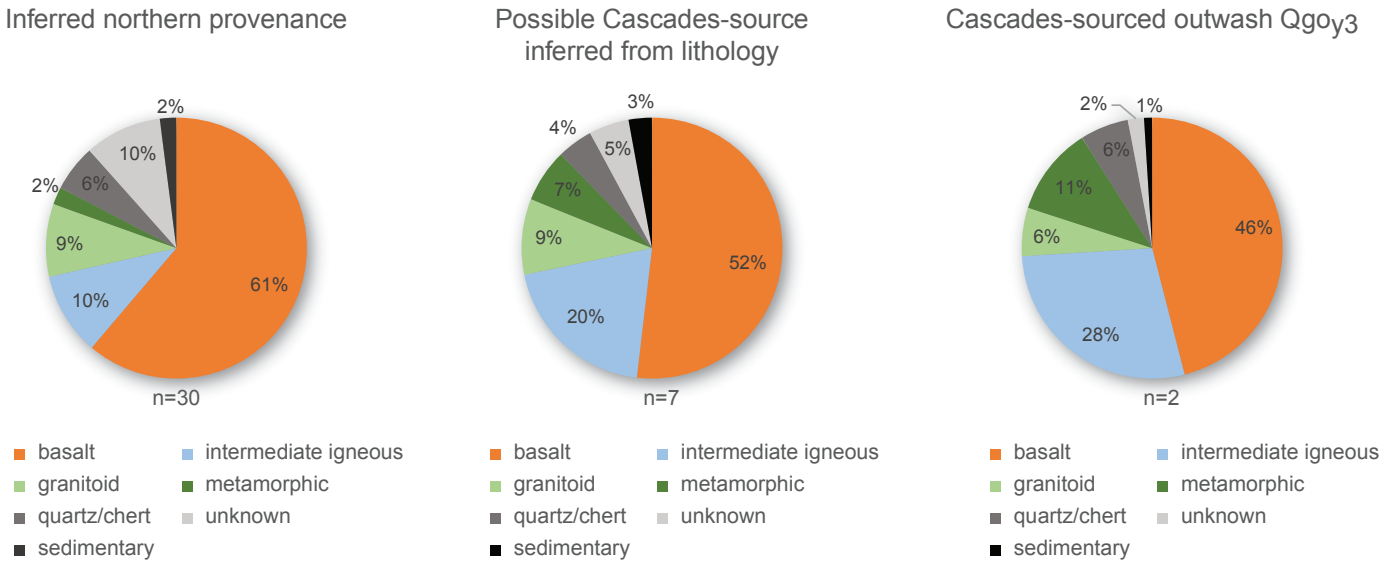

Figure 1. Pie charts showing clast lithologies from unlithified deposits. Charts were constructed from averages of (n) clast counts in each sample group (see Table DS5 for individual counts). Clast counts with fewer than 50 clasts were excluded from the pie charts. Cascades-influenced sediment in the Littlerock quadrangle is defined by unit Qgoy3. Northern-sourced and possibly Cascades-sourced groups are both inferred from the clast counts.

Qgo$_{y3}$ **Vashon recessional outwash, Yelm lobe**—Sandy pebble gravel; pale gray, locally stained pale yellow to orange-tan; lightly weathered, with most weathering rinds less than 2 mm thick; loose; distinguished from other Vashon outwash in the map area by its higher andesite content (indicative of Cascade Range provenance), a correspondingly lower basalt content (Fig. 1), geographic restriction to a relatively elevated (early recessional) set of terraces near the southeast map corner, and by relative abundance of rocks—two clast counts revealed 32% (site C17) and 24% (site C16) intermediate to felsic igneous rocks, likely of Cascade Range provenance. Unit Qgo$_{y3}$ is adopted from Walsh and Logan (2005) and Logan and others (2009), who attributed this outwash to the 'Yelm lobe' of Vashon ice and associated outwash terraces to the Tanwax Creek–Ohop Valley flood (Pringle and others, 2000; Pringle and Goldstein, 2002).

Qgic **Vashon ice-contact deposits**—Patchy lodgment till, ablation till, flow till, and ice-proximal outwash of all sizes in varied amounts; pale gray or surficially stained tan to reddish brown; lightly to moderately weathered with most weathering rinds less than 2 mm thick; loose to compact; clasts mostly well rounded but ranging to angular; sand angular to well rounded; poorly sorted to well sorted; massive to bedded. Clasts are northern-sourced (Fig. 1) with ~50–70% basalt, ~10% each of granitic and intermediate igneous rocks, and lesser amounts of high-grade metamorphic and other rocks. Fluted to chaotic topography, kettles, eskers, varied compaction, and varied texture indicate deposition in contact with at least partly stagnant ice (Haugerud, 2009; Polenz and others, 2009, 2010). Unit Qgic resembles unit Qgim but unlike that unit is not specifically interpreted as ice-marginal moraine. Unit Qgic overlies Vashon advance outwash and older deposits. It is locally overlain by units Qa, Qp, and Vashon recessional outwash. Divided into:

Qgim **Vashon terminal moraine**—Patchy till, flow till, and ice-proximal outwash of all sizes, in varied amounts; pale gray or surficially stained tan to reddish brown; lightly to moderately weathered, with most weathering rinds less than 2 mm thick; mostly loose but ranging to compact; clasts mostly well rounded but ranging to angular; sand angular to well rounded; poorly sorted to well sorted; massive to bedded. Clasts are northern-sourced (Fig. 1) with ~50–70% basalt (generally increasing upslope along the edge of the Black Hills), ~10% each of granitic and intermediate igneous rocks, and lesser amounts of high-grade metamorphic and other rocks. Chaotic topography, kettles, eskers, varied compaction, and varied texture indicate deposition in contact with stagnant ice. Unit Qgim resembles unit Qgic but is less commonly fluted and more likely to be loose. Unlike unit Qgic, it is specifically interpreted as ice-marginal moraine. Unit Qgim overlies Vashon advance outwash and older deposits, and is locally overlain by units Qa or Qp, or Vashon recessional outwash units.

Qge **Vashon esker**—Pebbles and sand; medium gray; lightly to moderately weathered, with most weathering rinds less than 2 mm thick; mostly loose; clasts well rounded; well sorted;

distinctly channel-bedded in most exposures, with beds commonly oversteepened because source water, confined beneath ice, locally flowed uphill; northern-sourced clasts (granitic and high-grade metamorphic clasts) are readily apparent, but no clast counts were completed from the unit. Unit Qge was deposited by subglacial, supraglacial, or englacial meltwater and is found amid or adjacent to units Qgic and Qgim. Unit Qge was mapped by its distinctive sinuous hill landforms, but sedimentary characteristics were confirmed where possible.

Qgt **Vashon lodgment till**—Compact diamicton; matrix-supported with clasts ranging from pebbles to boulders; matrix of sand, silt, and clay in varied amounts; light gray where fresh, ranging to light brown with rust staining where basalt-rich or surficially weathered; lightly to moderately weathered and, due to low permeability, usually less weathered than other Vashon-age deposits; compact to very compact, with little to no porosity; varied particle size from boulders to clay; clasts angular to well rounded; massive or stratified; mostly northern-sourced (Fig. 1) with ~50–70% basalt, ~10% each of granitic and intermediate igneous rocks, and lesser amounts of high-grade metamorphic and other rocks. Most deposits are 2–10 ft thick, although some locally pinch out. Well records suggest thickness may locally reach as much as 100 ft. Where well-developed, unit Qgt forms a solid, concrete-like layer. Where disturbed due to construction, loose diamicton will usually still contain clods of hard and compact lodgment till. Poorly developed sections of lodgment till may be more porous, less compact, and not laterally extensive. Where recognized, such areas were mapped as unit Qgic. Unit Qgt overlies units Qga, Qgag, and older deposits. Unit Qgt is mapped mainly within the fluted lowlands and Black River valley. The advancing Cordilleran ice sheet deposited lodgment till directly at the base of the ice. Unit Qgt usually is in sharp, unconformable contact with underlying units Qga, Qgag, or older deposits. Unit Qgt is overlain by unit Qgo or postglacial deposits.

Qga **Vashon advance outwash, undivided**—Cobble gravel, pebble gravel, and sand in varied amounts; pale gray, pale brown where basalt-rich or weathered, and red, orange, or yellow where surficially iron-stained; lightly to moderately weathered; compact; well sorted; well rounded; thin bedded to massive; northern-sourced (Fig. 1) with ~50–70% basalt, ~10% each of granitic and intermediate igneous rocks, and lesser amounts of high-grade metamorphic and other rocks. Unit Qga was deposited by proglacial meltwater during the MIS 2 (Vashon stade) advance of the Cordilleran ice sheet. It was then compacted by overriding ice. Unit Qga is stratigraphically above any pre-Vashon sediments, and is overlain along a sharp, unconformable contact by unit Qgt or Qgo; where overlain by unit Qgic or Qgim, the contact may be conformable. Locally divided into:

Qgaf **Vashon(?) advance outwash lake deposits**—Blue-gray or medium brown clay with sparse pebbles and little to no sand; clast weathering moderate to heavy; compact; bedding not apparent; clay-rich matrix and apparent dropstones suggest glaciolacustrine origin; isolated >1 m (3.28 ft) granitic boulders exposed as lag deposits along a stream channel may be dropstones or erratic boulders placed by overriding ice. Unit Qgaf is mapped only where ice apparently impounded a small lake along the east slope of the Black Hills (sec. 34, T18N R3W and sec. 3, T17N R3W), but unobserved similar deposits are likely in similar settings farther south. The unit also appears to comprise much of a landslide deposit (unit Qls) in sec. 33, T17N R3W, where exposures on the opposite (northern) side of the valley show the former presence of a Vashon advance lake by foreset beds in northern-sourced outwash (point unit Qga at clast count site C48). The beds contain mildly weathered clasts (Table DS5) beneath lodgment till that was mapped as part of unit Qgim. The age of unit Qgaf near the northern map boundary is uncertain: limited matrix weathering favors Vashon age; moderate to advanced clast weathering suggests pre-Vashon age but could also indicate older clasts picked up by ice from nearby substrate.

Qgag **Vashon advance outwash gravel**—Clast-supported pebble gravel, slightly sandy in some exposures, but usually containing little or no silt or clay except locally in the top 2–15 ft directly beneath till; pale gray, ranging to pale brown where basalt rich or weathered and to red, orange, or yellow where surficially iron stained; lightly to moderately weathered, with most weathering rinds <2 mm thick; usually compact, although, due to low cohesion, compaction can be difficult to confirm, and because well-sorted, well-rounded deposits can be mostly incompressible; clasts well rounded; moderately to well sorted; poorly bedded to unbedded. Unit Qgag can be found above any pre-Vashon unit. It is usually overlain along a sharp, unconformable contact by units Qgt or Qgo; where overlain by unit Qgic or Qgim, the contact may be conformable.

Pre-Vashon Glacial Deposits

Qpo2 **Possession-age distal outwash**—Northern-sourced sand and pebble gravel; tan to orange; moderately to heavily weathered; compact; locally lightly cemented; clasts subrounded to well rounded; sand beds well sorted, pebbly beds poorly to moderately sorted; bedding planar and gently crossbedded. Unit Qpo2 was identified only at Schematic Section 1, where it was deposited in a fluvial

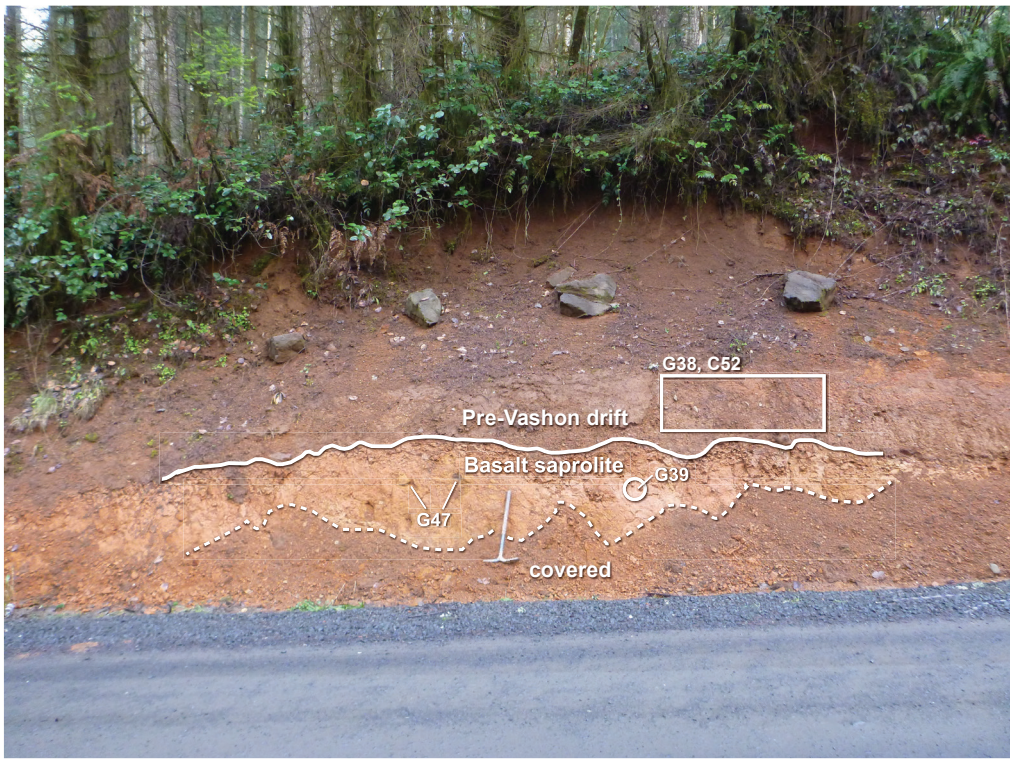

Figure 2. Roadcut showing sample locations for sites G47 (basalt corestones), G39 (basalt saprolite), G38 (pre-Vashon drift matrix), and C52 (clast count). The basalt boulders across the top of the outcrop are not in place and appear to have been moved by people with heavy machinery. Although largely clay, the drift is less weathered than the basalt-derived clay beneath it (see text).

channel setting with roughly south-directed paleocurrent. Optically and infrared-stimulated luminescence analyses from sand at age site GD2 near the top of the unit (Schematic Section 1; Tables M1 and B1) suggest deposition by south-draining meltwater during the Possession glaciation (MIS 4). Clast weathering and field relations are discussed below (see *Weathering*).

Qpo$_1$ **Pre-Possession outwash**—Northern-sourced pebble gravel, sand, and silt; dark brown or reddish brown; moderately to heavily weathered; loose; clasts subrounded to well rounded; moderately to well sorted; no bedding observed. Exposures were poor and limited to (1) an incised and truncated alluvial fan east of Waddell Creek that was likely proximal to pre-Vashon ice that deposited the surrounding undivided pre-Vashon drift (with similar clast weathering), and (2) a south-directed channel segment, truncated at both ends, at ~690 ft elevation west of Waddell Creek.

Qpf **Pre-Vashon glaciolacustrine deposits**—Gray clay and silt, with occasional pebbles; interpreted from well records and shown only in cross section. The unit predates unit Qoa (age site GD1). Unit age is otherwise unconstrained.

Qpd **Pre-Vashon drift**—Clay matrix–supported drift, locally pebbly, less commonly containing cobbles, sand, and rare boulders; clasts rounded but some grade to angular; ranges from soil consisting entirely of clay to weathered diamicton suggesting till; elsewhere, clay soil may have developed from glaciolacustrine deposits, outwash, or loess; pale brown to deep red; heavily weathered with weathering rinds on most clasts >2 mm; many deposits entirely saprolitized or weathered to clay soil. Where clasts are fresh enough to identify, clast counts suggest a northern-sourced assemblage (Fig. 1) with ~50–70% basalt, ~10% each of granitic and intermediate igneous rocks, and lesser amounts of high-grade metamorphic and other rocks, but we do not believe our data have ruled out the presence of some Cascades-sourced deposits. Compaction is not apparent in most exposures, but advanced weathering and soil formation may have masked or obliterated original compaction. Some exposures appear to be moderately to heavily weathered pebbles floating in red clay, but close inspection of the clay reveals that it was originally a diamicton, as at clast count site C52 (Fig. 2) and at site G51 (Fig. 3). XRD analysis of clay matrix samples revealed 36–37% (by weight) of halloysite, 29–40% quartz, 11–13% feldspar (albite and orthoclase), 2–13% goethite, and small but varied percentages of other minerals. Sample G38 (Table DS9) is an outlier that we mapped as unit Qpd based on our field examination. Its clay content does not clearly fit any mapping unit, and we are unsure how to interpret the combination of 63% halloysite, 10% quartz, and 3% magnetite in this sample. Unit Qpd overlies unit QEcf, Ev$_c$, or Em$_{2m}$ (Figs. 2 and 3).

Eocene to Quaternary Continental Deposits

QEcf **Terrestrial weathering clay**—Clay-rich soil and saprolite concealing underlying bedrock or sediment; mostly derived from basalt and locally contains corestones of basalt parent material or rare to common, well rounded, mostly moderately weathered, randomly distributed exotic clasts; red to reddish yellow and reddish brown or where saprolitic, locally variegated or mottled white, yellow, light lilac, red, and orange;

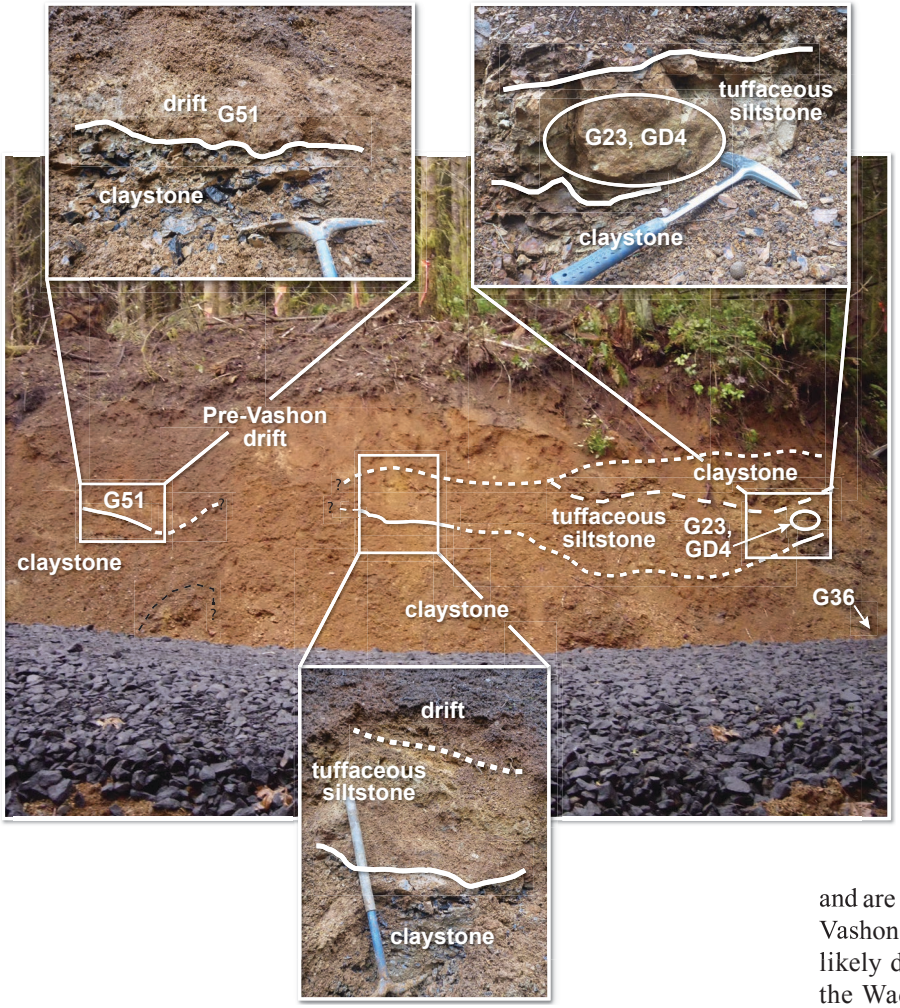

Figure 3. Roadcut showing sample locations for U-Pb date sample from site GD4 (tuffaceous sandstone of unit Em_{2m}) and geochemistry samples G23 (split from same tuffaceous sandstone), G36 (claystone of unit Em_{2m}), and G51 (pre-Vashon drift).

loose where bioturbated or affected by mass wasting, dense (but soft) where undisturbed; mostly structureless, locally hackly; core-stones commonly spheroidally weathered (onionskin texture; Fig. 4); some exposures reveal faint to distinct, prismatic, columnar, subangular or angular blocky soil structure. Minerals from parent rocks are almost completely decomposed. XRD analysis of clay soil and saprolite that were field-interpreted as basalt-derived revealed 44–80% (by weight) of halloysite and 15–26% goethite. A sample from geochemistry site G31 (Table DS9) is an outlier that we mapped as unit QEcf on the basis of our field examination. Its clay content does not clearly fit any map unit, and we were unsure how to interpret its combination of 38% quartz, 24% chlorite, 14% feldspar, 10% gibbsite, smaller amounts of muscovite/illite and goethite, and 0% halloysite.

Less common, and commonly forming a <10 ft thick surficial drape over basalt-derived clay, are clays derived from pre-Vashon drift (found only downslope of the pre-Vashon ice limit and the pre-Vashon lake Waddell shore). Where glacial diamicton origin of the clay could be identified and appeared extensive enough to show at map scale, it was mapped as unit Qpd (Figs. 2 and 3), but it has a distinctly different major element and clay mineral content than does clay derived from basalt (see also unit Qpd; Tables DS9 and DS7; *Geochemistry* below). The thickest observed exposure of clay extended at least 30 ft below the surface (significant site S6, sec. 25, T17N R4W), although some exposures reveal only a few feet of clay above weathered but intact basalt. (Where exposures were mostly bedrock within no more than 5 ft of the surface, we generally mapped the bedrock as surface unit.) We did not observe a systematic variation in clay thickness related to geography or slope; some of the thickest clay exposures were on moderately steep midslope surfaces. In the Waddell Creek watershed, scattered, well-rounded, exotic pebbles are locally present west of the pre-Vashon ice limit up to 800 ft elevation (just below former lake shoreline on map). The pebbles appear to be randomly distributed in the upper few feet of structureless clay, with no apparent stratification (Bretz, 1913) and are more weathered than road aggregate (for which Vashon Drift pebbles are commonly used). They are likely dropstones from a pre-Vashon glacial lake in the Waddell Creek basin and may have settled into pre-existing basalt-derived clay.

Tertiary Volcanic and Sedimentary Bedrock

Em_{2m} **McIntosh Formation (middle Eocene)**—Claystone with tuffaceous interbeds of siltstone and sandstone; tan to dark olive brown; lightly to heavily weathered; moderately lithified; silt- and sand-sized particles angular to rounded; poorly sorted. Although some outcrops faintly reveal 30–50 cm (11.8–19.7 in.) thick beds, most exposures are heavily weathered and reveal no sedimentary structure. XRD analysis indicates 65–75% (by weight) nontronite, a smectite clay. Other minerals in the clay-sized fraction include 17–20% feldspar and minor amounts of quartz, mica, heulandite, anatase, apatite, and goethite. Silt- and sand-sized clasts in distinctly tuffaceous beds include quartz, albite, orthoclase, sanidine, and minor amounts of varied mafic minerals; varied clays are likely secondary. Cements in the siltstones and sandstones are calcite or mica/clay; where the matrix is clay it is unclear if the clay is depositional or secondary. Nontronite is associated with high pH values and alteration in marine environments and thus suggests submarine alteration. Some samples of the claystone contain silt to fine sand-sized bioclasts that

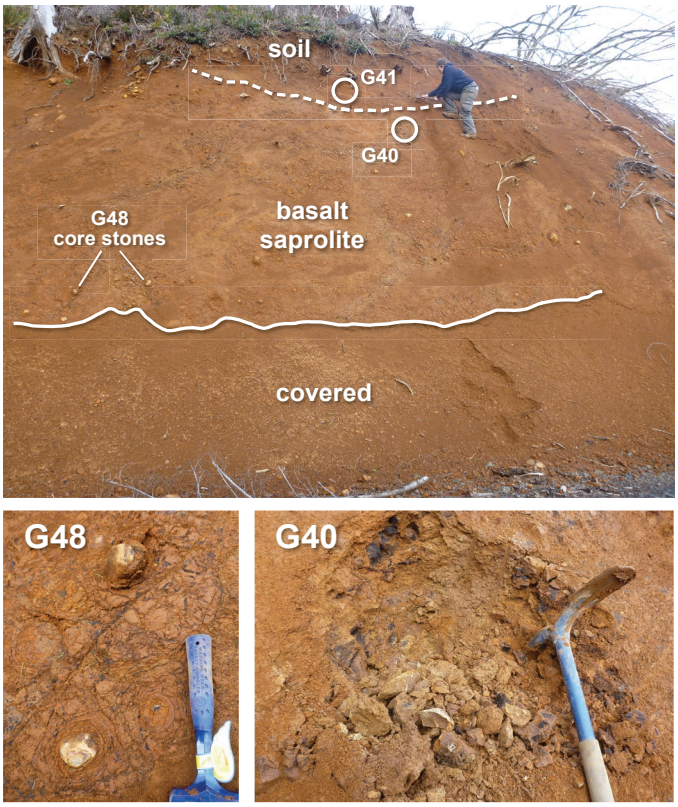

Figure 4. Roadcut with clay at geochemistry sites G48 (basalt core-stones), G40 (basalt saprolite), and G41 (basalt-derived clay soil).

are likely foraminifera. We recognized unit Em_{2m} only near the south end of the map area at and near age site GD4 and northwest thereof. We observed no overlying bedrock and suspect that unit Em_{2m} systematically overlies unit Ev_c. The tuff-rich sedimentary rocks of unit Em_{2m} fit Snavely and others' characterization of the McIntosh Formation, but would in our experience be uncommon in Crescent Formation. We interpret unit Em_{2m} in the map area as the stratigraphic base of the McIntosh Formation, owing to its apparent presence as relatively thin drape of sedimentary rock over Crescent Formation basalt and an approximately 47.4 Ma U-Pb age (Tables M1, A4, and DS3; Fig. 3) for a bed of slightly reworked airfall tuff within the unit. This age is consistent with a close maximum limiting age for the base of the McIntosh Formation and is therefore a marker for the regional transition from Siletzia terrane basaltic volcanism, which from north to south includes the Metchosin igneous complex, Crescent Formation, and Siletz River Volcanics (Wells and others, 2014; Eddy and others, 2017), to marine sedimentation (Armentrout and others, 1983; Babcock and others, 1994; Wells and others, 2014; Eddy and others, 2017). The age of unit Em_{2m} is further discussed below (see *Ages of Deposits and Paleoenvironmental Interpretations*).

Evb **Basalt (early middle Eocene)**—Aphanitic basalt; dark gray, weathers to medium gray; moderately dense; not vesicular; fine grained, porphyritic, and trachytic; fine-grained groundmass consists of 50–70% euhedral plagioclase and 20–35% pyroxene, with accessory opaque minerals; phenocrysts were likely olivine and have been entirely altered to iddingsite; some chlorite alteration is present, but very little zeolite. A new 46 Ma $^{40}Ar/^{39}Ar$ date for this unit (GD3; Tables M1, A3, DS1, DS2) and petrographic and geochemical trends contributed to our decision to separate unit Evb from the Crescent Formation and nearby unit Eig of Logan and others (2009)(see *Ages of Deposits and Paleoenvironmental Interpretations* and *Geochemistry*). Unit Evb cores a small hill at the east edge of the quadrangle along the boundary with the Maytown quadrangle (GD3; geochemistry sample site G8).

Ev_c **Crescent Formation (early to middle Eocene)**—Aphanitic basalt flows, with rare marine claystone interbeds of negligible thickness, except where separately mapped as subunit Em_{1c}?; dark gray or black; lightly to heavily weathered; massive; commonly vesicular with vesicles ranging from <1 mm–3 cm (0.04–1.2 in.) in diameter; aphanitic groundmass with fine- to coarse-grained phenocrysts of plagioclase (25–60%) and pyroxene (25–50%); accessory minerals include opaque minerals, olivine, and devitrified glass; some samples contain abundant zeolite, chlorite, and (or) clay alterations. Geochemistry and petrography suggest two groupings within Crescent Formation basalt in the Littlerock quadrangle (see below and *Geochemistry*). Although Crescent Formation basalt appears to core all of the Black Hills, we mapped it only where intact bedrock was exposed at or near the surface; most bedrock was concealed by highly weathered soil and saprolite (unit QEcf). Although flow contacts and rare sedimentary interbeds in the Black Hills have yielded marine microfossils (Pease and Hoover, 1957; Logan, 1987; Walsh and others, 1987; Squires and Goedert, 1994; Rau, 2004; Logan and Walsh, 2004; Polenz and others, 2016), biostratigraphically constraining assemblages have proven hard to find. Fossil content of sedimentary rocks mapped as unit Em_{1c}? is discussed below (see *Ages of Deposits and Paleoenvironmental Interpretations*). Fossil site GD9 (sec. 32, T17N R3W) was included with unit Ev_c because it represents only minor void-space fills in a partly brecciated vesicular basalt exposure. Contact relations of unit Ev_c with nearby exposures of sedimentary rock (units Em_{1c}? and Em_{2m}) were not exposed; along Waddell Creek, identification of unit Em_{1c}? and its interbedded relationship with unit Ev_c remain tentative, as does the onlapping relationship of unit Em_{2m} near the southern map edge.

Basalt in the vicinity of unit Em_{2m} near the southern map edge slightly differs geochemically and petrographically from basalt farther north. The transition between the two groups is around Mima Creek, where basalt at low elevations is geochemically and petrographically similar to the northern group (sites G25 and S3). All basalt south of the creek, as well as site G1, is in the southern group (see *Geochemistry* and Fig. 5). The

distribution of these samples suggests that the southern group may be stratigraphically above the northern group.

Snavely and others (1958) mapped basalt near the south end of the Black Hills, including in parts of the Littlerock quadrangle, as volcanic facies of the McIntosh Formation. In contrast, Pease and Hoover (1957) mapped all Black Hills basalt within their map area west and southwest of the Littlerock quadrangle as Crescent Formation. According to Timothy Walsh (WGS, oral commun., 2016), Weldon Rau later opined that all basalt formerly mapped as McIntosh Formation in the Black Hills is instead Crescent Formation. This reassessment is consistent with a comment Rau (2004) made regarding rocks at age site GD19 (Fig. M1; Table M1). We note that despite small but systematic differences relative to basalt farther north in the Black Hills, the basalt near the southern map edge is well within the range of Crescent Formation chemistry. We therefore follow Pease and Hoover (1957), Logan (1987, 2003), Walsh and others (1987), Schasse and others (2003), Logan and Walsh (2004), and Polenz and others (2016) in mapping all basalt in the Black Hills as Crescent Formation.

Em1c? **Crescent Formation(?) marine sedimentary rocks (early to middle Eocene)**—Claystone; gray-blue to olive brown; lightly to moderately weathered; moderately to well lithified; mostly clay with sparse foraminifera and silt-sized lithic fragments; prominent to faint bedding, 1–3 cm (0.4–1.2 in.) thick; unit thickness is unclear, but at least 22 ft was observed at fossil sample sites GD5 and GD6 along Waddell Creek near the eastern edge of the Black Hills (sec. 33, T17N R3W). Biostratigraphic analysis of these sediments shows they are marine and of Eocene age (see *Ages of Deposits and Paleoenvironmental Interpretations*). No contact relations were observed at sites GD5 and GD6, but the sedimentary rock at site GD8 (2,300 ft southeast of sites GD5 and GD6) appears to be deposited atop altered basalt that is chemically similar to Crescent Formation and has been mapped as such. However, the full stratigraphic relationship between these sedimentary rocks and the surrounding Crescent Formation remains unclear, and these sedimentary rocks may be interbedded with, onlapping on, or thrust beneath the Crescent Formation.

AGES OF DEPOSITS AND PALEOENVIRONMENTAL INTERPRETATIONS

Bedrock Units

CRESCENT FORMATION

Several Ar dates from Crescent Formation basalt in the Black Hills range between ~55 and ~50 Ma (Czajkowski, 2016). A high-precision U-Pb analysis of zircons dates a tuffaceous sedimentary interbed in the northern Black Hills to 49.729 ±0.014 Ma (Polenz and others, 2016; Eddy and others, 2017). Regionally, Crescent Formation and associated rocks of the Siletzia terrane (Metchosin igneous complex and Siletz River Volcanics) yielded U-Pb and Ar dates from 56 to 48.4 Ma (Wells and others, 2014; Eddy and others, 2017), with some undated Siletzia sections both below and above (Ken Clark, Univ. of Puget Sound, oral commun., 2017). A new 47.4 ±1 Ma U-Pb date on zircon crystals from a reworked airfall tuff bed in sedimentary rocks that we mapped as McIntosh Formation near the south end of the Littlerock quadrangle (age site GD4; Tables M1, A4, and DS3; Fig. 3) provides a close maximum limiting age for the McIntosh Formation just upsection of Crescent Formation. This suggests that the transition from Crescent Formation basalt deposition to McIntosh Formation marine sedimentary rock deposition occurred between 48.364 ±0.036 and 47.4 ±1 Ma.

The above-suggested time of transition from Crescent Formation to McIntosh Formation is consistent with biostratigraphy-based estimates for this transition (Armentrout and others, 1983). Biostratigraphic data from within and near the map area are consistent with but do not further constrain the above-stated Crescent Formation age ranges. Foraminifera we obtained from sedimentary rocks at age sites GD5 and GD6 suggest Ulatisian or lower Narizian age (E. Nesbitt, Burke museum, written commun., 2017), compatible with foraminiferal assemblages from both the Crescent and McIntosh Formations. This is consistent with prior assertions of middle Eocene age for foraminiferal assemblages 3.5 mi southwest of the map area (age site GD19; Pease and Hoover, 1957; Rau, 2004) and Ulatisian stage (also middle Eocene age) at Rock Candy Mountain 1 mi north of the map area (age site GD20; Rau in Globerman and others, 1982; Rau, 2004; Logan and Walsh, 2004).

Most Crescent Formation basalt exposures in the Littlerock quadrangle are small and weathered. To the extent that they permitted characterization, they revealed massive to columnar and vesicular basalt. We found no definitive evidence of pillows. Only two areas revealed more than a trace of sedimentary rocks: one being at and near age sites GD5 and GD6 in and along the active channel of Waddell Creek (sec. 33, T17N R3W), the second near the south edge of the map area, where we followed Snavely and others (1958) in mapping sedimentary rocks as McIntosh Formation (see *McIntosh Formation* below). Crescent Formation rocks at biostratigraphy sites GD5 and GD6 (sec. 33, T17N R3W) are marine sedimentary claystone from neritic (<200 m) water depth and yielded a low-diversity assemblage of middle Eocene foraminifera (Tables M1 and DS4). The samples lacked index species for benthic foraminiferal zones and contained planktonic species that are temporally wide-ranging. The samples could be from Rau's (1958, 1981) *Vaginulinopsis vacavillensis*

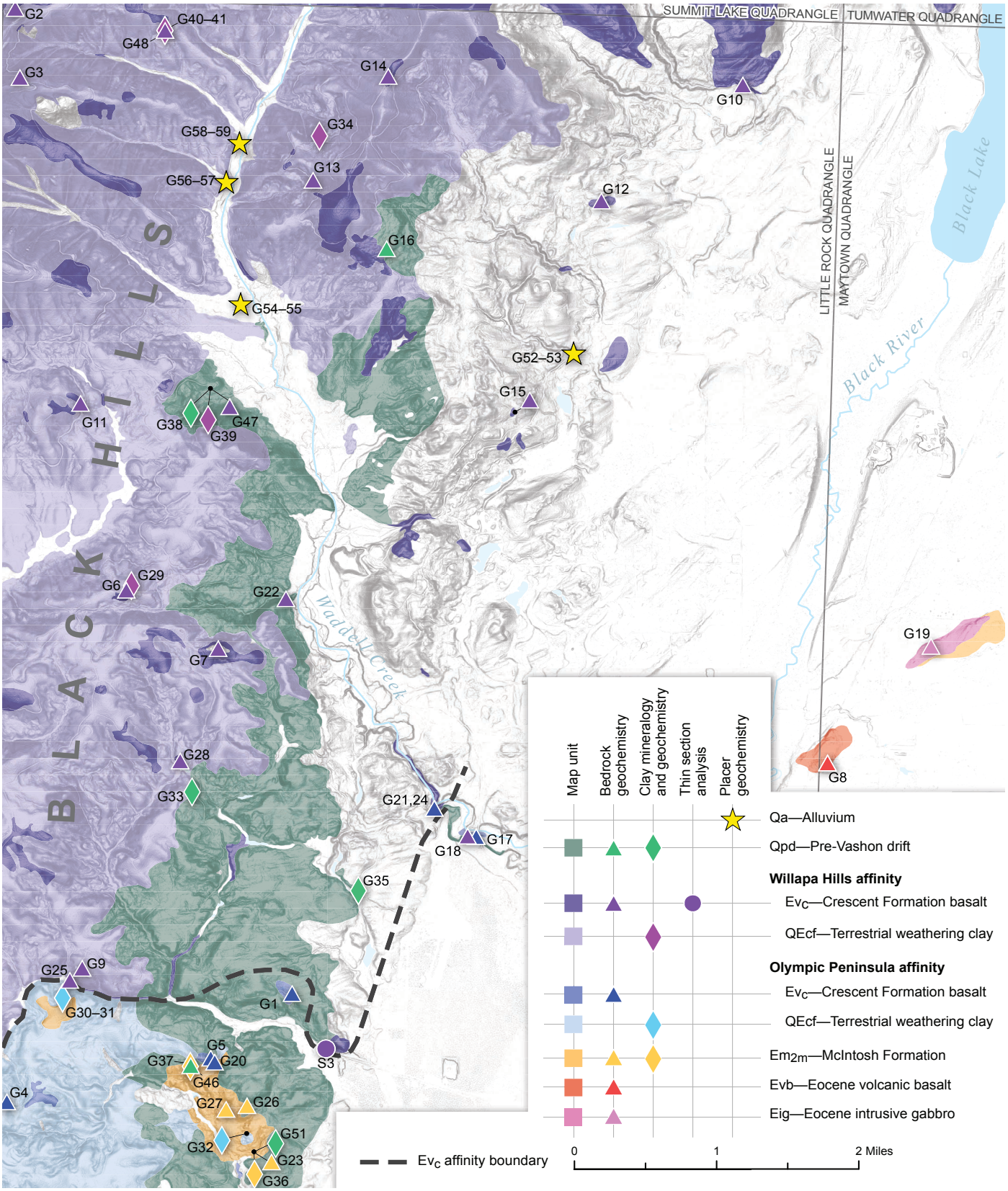

Figure 5. Simplified geologic map showing geochemistry sample locations, geologic units, and analysis type. Crescent Formation basalt can be subdivided into two groups based on geochemical and petrographic characteristics; see text for discussion. The dashed line shows the inferred contact between these two Crescent sub-units.

zone (Ulatisian Stage) up through *Uvigerina* cf. *U. yazooensis* zone (lower Narizian of Mallory, 1959)(E. Nesbitt, written commun., 2017). This foraminiferal content is consistent with prior interpretations that the Crescent Formation in the central and southern Black Hills was deposited in a shallow marine to subaerial setting (Table M1, age site GD20; Rau in Globerman and others, 1982; Rau, 2004; Squires and Goedert, 1994; Walsh and Logan, 2004).

UNIT Evb

Basalt at $^{40}Ar/^{39}Ar$ age site GD3 (~46 Ma; same rock as geochemistry site G8)(Figs. M1 and 5; Tables M1, A3, DS1, and DS2) was mapped by Logan and others (2009) as unit Eig, but is laterally continuous with nearby basalt mapped as unit Evb in the Littlerock quadrangle. We interpret basalt on both sides of the quadrangle boundary as unit Evb instead of the gabbro unit Eig of Logan and others (2009) because: (1) the 46 Ma date from GD3 suggests an older rock than the ~39 Ma date reported by Walsh and Logan (2005) for their unit Eig in the East Olympia quadrangle about 6 mi east of the Littlerock quadrangle. (2) All bedrock exposures we found at GD3 and elsewhere on the same hill (including the part of the hill within the Littlerock quadrangle) are fine-grained basalt. Timothy Walsh (WGS, oral commun. 2016) noted that Walsh and Logan (2005) and Logan and others (2009) also found basalt in association with the gabbro of their unit Eig; we never found gabbro. (3) We revisited geochemistry sample loc. 1 of Logan and others (2009, their unit Eig) and sampled basalt nearby (geochemistry site G19, Fig. M1; Fig.5). Our sample from site G19 matches the geochemistry of Logan and others' sample of unit Eig from the same hill; both also resemble unit Eig where it was dated to ~39 Ma farther east (Fig. M1; Walsh and Logan, 2005). However, the sample from site G8 (Fig. M1; Fig. 5) geochemically differs slightly from those samples (see *Geochemistry*). Petrographic sample review shows that unit Evb is consistently fine grained and trachytic, with a greater percentage of plagioclase that is pristinely euhedral, whereas unit Eig of Logan and others (2009) farther east is medium to coarse grained, ~40% plagioclase and 20% pyroxene with most grains broken and embayed. These distinctions motivated our reassignment of the basalt at age site GD3 to unit Evb.

Aside from separating the rocks at and near age site GD3 from unit Eig of Logan and others, our 46 Ma age estimate for GD3 also suggests that the basalt at this locality is not Crescent Formation. The 46 Ma age is somewhat younger than all above-mentioned age constraints on the Crescent Formation, although outside the Black Hills, rocks mapped as Crescent Formation have yielded $^{40}Ar/^{39}Ar$ dates that are much younger still (Czajkowski, 2016). However, at least some of those younger dates appear to be reset (Randall Babcock, Western Wash. Univ., oral and written commun., 2012), and as far as we know, no U-Pb analyses have produced comparably young age estimates anywhere in Crescent Formation.

The 46 Ma age at site GD3 is also younger than at age site GD4 (~47.4 Ma; Tables M1, A4, and DS3; Fig. 3) from McIntosh Formation sedimentary rocks that are upsection of Crescent Formation near the south end of the map area. This adds further support for mapping the basalt at age site GD3 as something other than Crescent Formation, although chemical similarities suggest that Crescent Formation (unit Ev_c) and Logan and others' (2009) unit Eig all share the same mantle source (see *Geochemistry*).

The ~46 Ma age at age site GD3 suggests temporal association with the McIntosh and maybe early Northcraft Formations (for which ages have been determined from biostratigraphy, supplemented herein by age site GD4), but we consider both formations unattractive matches for the basalt at age site GD3. Basalt has been mapped as part of both formations, although for the McIntosh Formation, this basalt is restricted to the southern flanks of the Black Hills (Snavely and others, 1958), where Pease and Hoover (1957) and more recent studies (including ours, Logan, 1987, and Walsh and others, 1987) have instead mapped basalt as Crescent Formation. The Northcraft Formation is mostly younger and differs chemically from both Crescent Formation and unit Eig of Walsh and Logan (2005) and Logan and others (2009)(see *Geochemistry*, Fig. 11C).

McINTOSH FORMATION

Zircons from age site GD4 (sec. 8, T16N R3W; Fig. 3) yielded a laser ablation U-Pb date of 47.35 ±0.21 Ma (Tables M1, A4, and DS3). The lab cautioned that the large number of zircons (50) inappropriately reduces the stated error, and true error is likely about 1 Ma (Table D1). The age is therefore ~48.4–46.4 Ma.

For the sedimentary rocks at and near age site GD4, we interpret the well-sorted, highly tuffaceous sandstone from which the zircons were sampled as slightly reworked airfall tuff. We infer that the zircon crystals likely were extruded in a single eruption—followed within hours to days by sediment deposition. We characterize the age as a close maximum limiting age of sediment deposition in the Littlerock quadrangle because some or all of the analyzed zircon crystals may have formed prior to the eruption and may therefore be older than the age of eruption.

Alternatively, if the sandstone bed we sampled was a distal deposit from an ashflow, zircon extrusion could be spread over multiple eruptions, followed by an event (for instance, a volcanic sector collapse landslide) that mixed rocks from multiple eruptions and deposited some of this mix in the single sandstone bed we sampled in the Littlerock quadrangle. In that scenario, the sedimentary host rock would clearly be younger than the ~48.4–46.4 Ma zircons within it, although perhaps also not much younger. We think the latter scenario unlikely because: (1) the 50 zircon analyses ages are tightly clustered around a single peak, (2) the tuffaceous sandstone bed is no more than ~50 cm (~20 in.) thick and distinct from the finer-grained sedimentary beds above and below, (3) the deposit is well sorted, (4) particles in the tuffaceous sandstone are only slightly rounded, and (5) overall evidence for sedimentary texture is limited, with only isolated lithic fragments. We interpret the limited particle rounding and incorporation of lithic fragments as evidence of minor detrital reworking, but the deposit fundamentally appears to be the product of an airfall tuff.

We believe that we collected the sample for age site GD4 very close to the base of the sedimentary rock section above basalt near the south end of the Littlerock quadrangle and infer that the age essentially marks the basal age of the McIntosh Formation at 47.4 ±1 Ma.

We interpret the middle Eocene age of the zircons sampled at age site GD4 as consistent with either the age of the McIntosh

Formation or very late Crescent Formation. We know of no prior radiometric ages from the McIntosh Formation, although prior biostratigraphic age control (Snavely and others, 1958, 1959; Rau, 2004) has yielded similar age estimates for the base of the McIntosh Formation (Armentrout and others, 1983). Radiometric and fossil age control for the Crescent Formation is further discussed above. Whereas Pease and Hoover (1957) interpreted the young end of the Crescent Formation as coeval with McIntosh Formation, Snavely and others (1958) asserted that the McIntosh Formation overlies the Crescent Formation. Both mapping teams agreed that McIntosh Formation is younger overall than Crescent Formation. We mapped the sedimentary rocks near the south end of the Littlerock quadrangle, including at age site GD4, as McIntosh Formation because:

1. They fit Snavely and others' (1958) description of McIntosh Formation as a tuffaceous marine deposit. The claystone is rich in nontronite, which commonly forms in marine environments (Dixon and Weed, 1989). We identified strongly tuffaceous beds at four sites (including geochemistry sites G26, G27, G30, and G23; Fig. 3, GD4) amid mostly very weathered exposures that cover no more than ~0.5 mi² and probably do not add up to much stratigraphic section. Petrographic examination further revealed that all other McIntosh Formation samples of siltstone and sandstone in the map area are also tuffaceous. In addition, the simple presence of a notable thickness and areal extent of sedimentary rocks is atypical of Crescent Formation in the Black Hills.

2. It is our (unproven) impression that these sedimentary rocks systematically overlie basalt, consistent with a succession from Crescent Formation to McIntosh Formation.

3. Snavely and others also mapped McIntosh Formation at the south end of the Black Hills (Snavely and others, 1958). However, whereas Snavely and others mapped all rocks (including basalt) in this area as McIntosh Formation, Pease and Hoover (1957) mapped adjacent basalt and sedimentary interbeds farther west as Crescent Formation. To our knowledge, neither mapping team had geochemical data from the area. Biostratigraphic data referenced by Pease and Hoover about 3 mi southwest of the Littlerock quadrangle was characterized as "middle Eocene" (age site GD19, sec. 27, T16N R4W). We suspect this refers to record no. 119 of Rau (2004), who identified his sample "BG51-5" from 2,700 ft west and 900 ft north of the SE cor. of sec. 27, T16N R4W as "lower McIntosh Formation, now considered Crescent Formation". Our new 47.4 ±1 Ma U-Pb date (age site GD4) from zircon in a reworked airfall tuff bed near the southern edge of the Littlerock quadrangle is consistent with the biostratigraphic age of the McIntosh Formation, although the date may also fit the young end of the Crescent Formation.

4. Our petrographic analysis of samples of weathered sedimentary rock and soil from near the southern quadrangle edge revealed that these weathered rocks and soil commonly include plagioclase. In contrast, we found little or no preservation of plagioclase in soils and saprolitic bedrock exposures derived from basalt. Although syndepositional alteration of basaltic samples may have played a role in alteration of plagioclase in the basalt, surficial exposure and initial weathering of the basalt may also have preceded deposition of the overlying sedimentary rock. A possible interlude of subaerial basalt surface emergence and weathering is supported by suggestions that Eocene accretion of the Siletzia terrane was accompanied by uplift, shortening, and exhumation (Groome and others, 2003; Johnston and Acton, 2003; Wells and others, 2014; Eddy and others, 2017). This could have led to emergence (and thus surficial weathering) of Crescent Formation basalt in the Black Hills, at least some of which appears to have been initially deposited in a shallow marine environment (see *Crescent Formation* discussion, above). Any such emergence would have been followed by enough subsidence to permit deposition of marine sedimentary rocks, such as the McIntosh Formation, on at least the peripheral parts of the Black Hills, starting ~47.4 ±1 Ma (age site GD4).

Quaternary Units

PRE-VASHON DEPOSITS

Most pre-Vashon sediments along the eastern flank of the Black Hills are interpreted as glacial deposits. Northern-sourced till, outwash and lake sediment were deposited along the eastern slope of the Black Hills during at least two southward incursions of the Cordilleran continental ice sheet into the map area—the most recent Vashon stade ice advance (MIS 2) and one or more earlier ice advance(s) of indeterminate age. Northern-sourced outwash of unit Qpo2 reached the map area during MIS 4 even though ice of the Possession glaciation did not. All other pre-Vashon drift dates to MIS 6 or earlier.

WEATHERING

The relative age of Quaternary units was assessed using clast weathering (Table DS5), mostly to gain a better sense of deposit ages, but also to provide some basis for comparison with assessments of clast weathering from prior studies in or near the map area (Carson, 1970, 1980; Colman and Pierce, 1981; Lea, 1984; Polenz and others, 2016). Matrix weathering observed in thin sections yielded similar assessments (Tables DS6 and DS5). Two distinct degrees of weathering were generally apparent in the field and were confirmed in both clast counts and matrix weathering. They are illustrated by the groupings in Fig. 6. Vashon-age and younger deposits generally contained fewer than 80 percent of clasts with rinds >0.5 mm, whereas 80–100 percent of clasts in pre-Vashon deposits had >0.5 mm rinds. Weathering of basalt clasts did not vary much from the weathering of a randomly selected mix of clasts of all lithologies (Fig. 7). The long tail on the mildly weathered end of Vashon Drift is due to inclusion of a sample from deep below the surface (clast count site C1, Table DS5; sec. 10, T16N R3W), where surficial weathering had little influence, and it illustrates that surficial weathering has left a mild but distinct imprint on Vashon Drift in the map area. The single dot marking a mildly weathered clast above the pre-Vashon drift is a sample of pre-Vashon lodgment till (clast count site C23) and illustrates how compaction and low

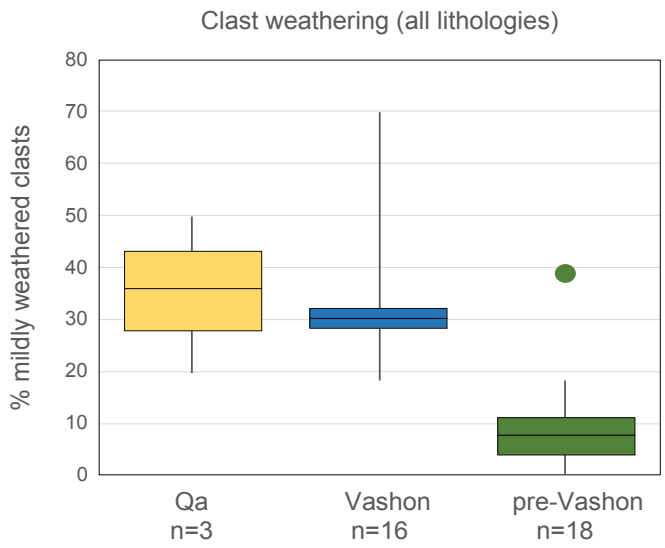

Figure 6. Range of clast weathering for unit Qa and Vashon and pre-Vashon glacial deposits. Glacial deposits were classified as Vashon or pre-Vashon based on multiple criteria. Clast counts with less than 20 percent mildly weathered clasts were initially classified as pre-Vashon ("Mildly weathered" clasts are those classified in clast counts as "fresh" or "rinds <0.5 mm", see footnotes to Table DS5). Age classifications were either confirmed or re-evaluated after petrographic examination of the matrix (deposit was classified as Vashon if the sand grains and small lithic clasts had little or no weathered rind). The classifications of Vashon or pre-Vashon age displayed here integrate clast weathering, matrix weathering, deposit morphology, outcrop stratigraphy, and geographic location. All clast counts are included in this diagram. See *Weathering* for a discussion of outliers.

permeability in lodgment till slows weathering. Despite the clear distinction between pre-Vashon age and younger deposits, the diagram under-represents the average weathering of pre-Vashon deposits because clast counts were mostly carried out where a field exposure left some doubt regarding the relative age of a deposit. In many pre-Vashon exposures, clast counts were not attempted because all pebbles appeared rotten, so there was no doubt of pre-Vashon age (and parent rock lithology could not have been confidently identified).

Some exposures of drift suggested a pre-Vashon age in the field, due to a clay-rich red matrix, but clast counts and matrix petrography revealed weathering more consistent with Vashon age (clast count sites C13 and C14). Typically, Vashon-age deposits lack such red clay. The matrix is gray or light tan and consists of clay-sized rock flour more than clay minerals. Petrographic analysis of the matrix from clay-rich drift with relatively lightly weathered clasts revealed an abundant red matrix clay, but little to no weathering rind on the sand-sized grains. Unambiguously pre-Vashon deposits reliably have weathering rinds on their sand-sized grains, or the sand fraction is weathered away completely. We interpret such clay-rich deposits with mild weathering of clasts and sand-sized matrix particles as likely Vashon Drift. The red clay in these deposits was probably incorporated into the drift matrix from already weathered local sources. Thin deposits near the edge of the ice would be particularly susceptible to incorporating locally sourced, highly weathered material into the matrix.

Comparison of relative weathering between different samples of pre-Vashon drift proved more complex. This is illustrated by comparison of three clast counts from units Qpo$_1$ (site C11) and Qpo$_2$ (sites C42 and C51; Schematic Section 1). All three samples revealed moderate to advanced clast weathering (Fig. 8; Table DS5). However, the clast count at site C42 contains a normal weathering distribution, whereas the weathering distribution at site C51 is distinctly skewed, with a strong peak of rotten clasts. Our field assessment of the exposure was that both clast count samples are from the same unit, with the sample from site C42 occupying a lower, more clast-rich facies. The skewed, nearly bimodal, distribution from site C51 could be an effect of incorporation of clasts recycled from a proximal source and already weathered at the time of deposition. If so, it illustrates inherited weathering resulting in clast weathering distributions that are not representative of the deposit age. Thus, we are unable to determine if the two counts represent deposits of different age, or deposits with a different amount of inherited weathering. Comparison of both clast counts with the count from site C11 in pre–MIS 4 unit Qpo$_1$ further adds uncertainty. Its weathering signal is intermediate between those from sites C42 and C51, with most clasts in site C11 moderately to strongly weathered, and few clasts either lightly weathered or rotten. This distribution may be indicative of a more evenly weathered deposit, with all clasts starting at the same point and weathering at a similar rate. We sampled at site C11 from a bedded outcrop of pebbles in a weathered clayey matrix at 695 ft

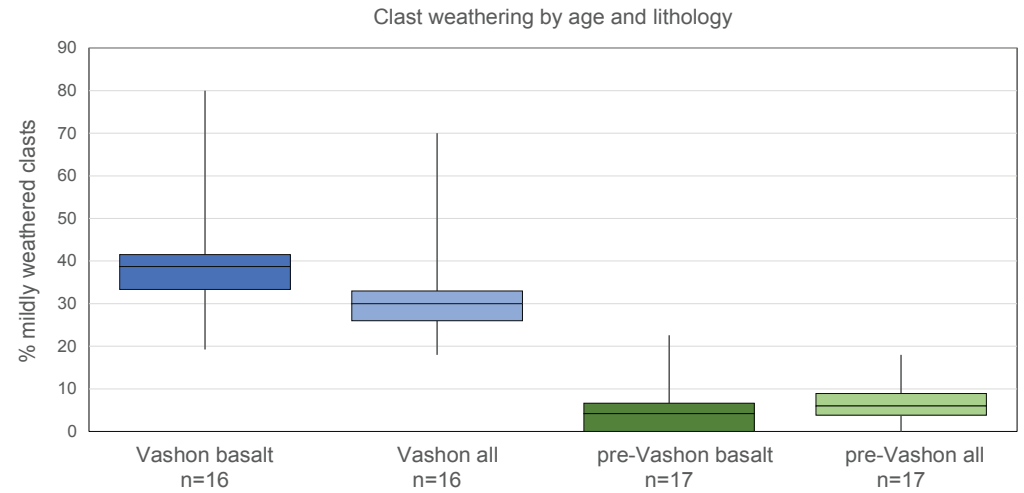

Figure 7. Weathering of basalt clasts vs. clasts of all lithologies. Focusing exclusively on basalt clast weathering did little to change the overall weathering signals in the Littlerock quadrangle.

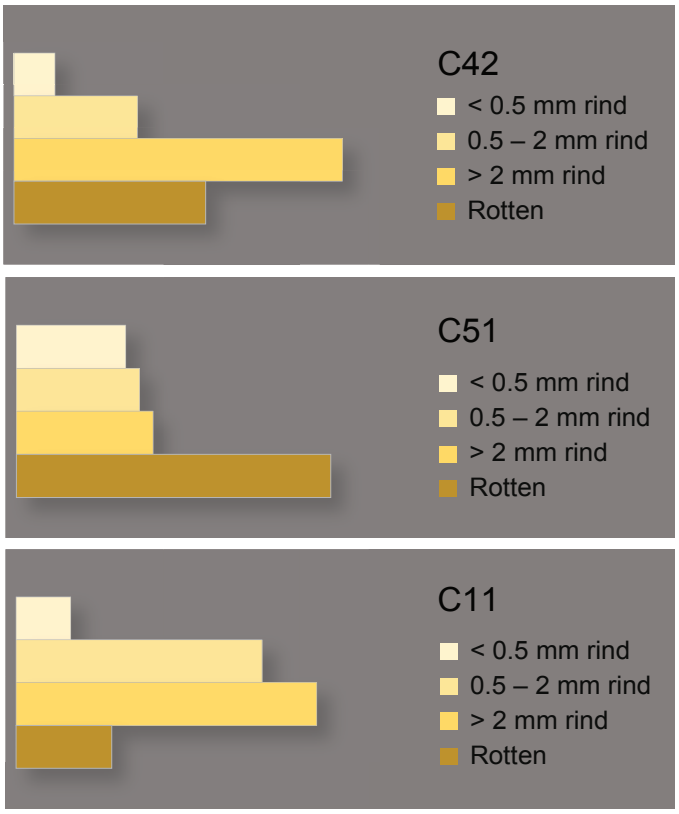

Figure 8. Clast weathering in units Qpo_1 (site C11) and Qpo_2 (sites C42 and C51.

elevation—higher than the Vashon ice limit in this part of the map area and therefore clearly older than MIS 4. Yet the clast count signal from site C11 is clearly less weathered than from site C42 and only slightly more weathered than at site C51. The message appears to be that, like soil weathering in general, clast weathering is an approximate game with large error margins for individual sites. All clast-weathering data should therefore be evaluated with caution, with attention also paid to stratigraphic context and other characteristics of the deposits.

INTERPRETATION OF WEATHERING AND MIS

Clasts and matrix in most of the pre-Vashon drift of the Littlerock quadrangle are very heavily weathered. Our clast counts underestimate the degree of unit Qpd weathering because we never attempted clast counts at many pre-Vashon sites where clasts and matrix were mostly or entirely clay. The degree of weathering can be used to estimate the deposit age relative to other exposures, but the weathering must be interpreted with caution; caveats include that weathering signals can vary for reasons other than deposit ages (as illustrated by the above discussion of clast counts from units Qpo_1 and Qpo_2), and that if a deposit was buried, subsequent weathering will be slowed, and the deposit will over time start appearing relatively younger. With these caveats, we note that pre-Vashon drift in the Littlerock quadrangle is generally far more weathered than previously dated units of pre-Vashon drift farther north in the Puget Lowland, such as the type section of the Salmon Springs Drift (~0.8 Ma)(Crandell and others, 1958) or the Clark Creek and Annas Bay Drifts of Carson (1980). The degree of weathering is similar to that of the Logan Hill Formation (Snavely and others, 1951, 1958), which some correlations suggest may range to Pliocene age (Lowry and Baldwin, 1952; Erdmann and Bateman, 1951). These comparisons suggest that, with the exception of meltwater-derived alluvium at low elevations (Schematic Section 1, sec. 34, T17N R3W), the pre-Vashon drift in the Littlerock quadrangle includes or consists entirely of deposits that may be older than most known exposures of pre-Vashon drift farther north in the Puget Lowland. We caution that the global MIS curve suggests that Quaternary ice advances were more pronounced during the most recent ~1 m.y. than earlier (Morrison, 1991), and it therefore seems tenuous to infer a significantly pre–Salmon Springs age for a Puget Lowland ice advance that exceeded the reach of the Vashon glaciation in the Littlerock quadrangle.

New luminescence dates at age site GD2 (Schematic Section 1; Tables M1 and A2) suggest that the fluvial section at that site is Possession-age sediment. The Possession glaciation (76–61 ka, Troost, 2016), is generally equated with a relatively weak global glaciation at MIS 4 (71–57 ka, Lisiecki and Raymo, 2005; Siddall and others, 2008) and is not thought to have extended south beyond Tacoma (Lea, 1984; Troost, 1999, 2016), more than 40 mi northeast of the Littlerock quadrangle. However, it dammed the Strait of Juan de Fuca and filled the Puget Lowland with water and (or) proglacial sediment. If the pre-Vashon topography was broadly similar to today's, this water, and perhaps also sediment, would have drained south into the Black River valley, thereby providing a mechanism for vigorous Possession-age erosion and sediment deposition in the lowlands of the Littlerock quadrangle. As discussed above, two clast counts from this unit (sites C42 and C51; Schematic Section 1) reveal clast weathering that is strikingly advanced relative to clearly older drift elsewhere in the Littlerock quadrangle. We speculate that average clast weathering at age site GD2 may be more advanced than would be representative of MIS 4–age drift because some or all clasts may be proximally derived from older deposits and retain an inherited clast-weathering signal. Such re-working of older deposits would be expected of sediment-starved lake drainage from the Puget Lowland north of Olympia during MIS 4 and would permit re-setting of the luminescence age of the sediment.

SEDIMENT PROVENANCE

We used clast counts from unconsolidated Quaternary deposits, petrographic examination of matrix material, and field observations to help assess sediment provenance. In clast counts, we recorded pebble lithologies as well as weathering.

Deposits sourced from the Black Hills are entirely composed of basalt and basalt-derived weathering products, except where soil is derived from unit Em_{2m} near the southern map limit. Such basalt dominance is illustrated by clast count site C6 from Mill Creek near the southwest map corner (sec. 12, T16N R4W) and was widely observed elsewhere. Northern-sourced clast assemblages were identified on the basis of Vashon Till and outwash, which are widespread and readily identifiable as the most recent glacial deposits in the east half of the Littlerock quadrangle; their clast content serves as guide to the interpretation of provenance of older drift. We used the mixed provenance of sediment in the well-documented Vashon recessional outwash unit Qgo_{y3} (Pringle and others, 2000; Pringle and Goldstein, 2002; Walsh and Logan, 2005; Logan and others, 2009) to define

clast assemblages that suggest a substantial contribution from the Cascade Range, although in the outwash of unit Qgo$_{y3}$, the clast assemblage is clearly tied to a northern-sourced ice incursion.

The northern-sourced deposits in the Littlerock quadrangle tend to include more than 50 percent basalt along with smaller fractions of granitoid and intermediate igneous rocks. Compared to northern-sourced deposits, unit Qgo$_{y3}$ is marked by a higher percentage of intermediate igneous clasts and a correspondingly reduced percentage of basalt clasts (Fig. 1). Both northern-sourced deposits and unit Qgo$_{y3}$ have roughly one-fourth of clasts consisting of a diverse mix of other rock types that are mainly northern-sourced, notably including metamorphic and sedimentary clasts.

Our clast counts suggest that some of the drift outside the unit Qgo$_{y3}$ terraces may be Cascades-sourced. We identified some drift samples within the Black Hills that have similarly low basalt content and high intermediate igneous content (Fig. 1). Many of these samples are highly weathered and likely pre-Vashon. These counts suggests that there may be Cascades-sourced drift within the Black Hills. Previous studies have documented that ice advances in the Cascade Range sent voluminous Cascades-sourced outwash into the Puget Lowland (Snavely and others, 1958; Lea, 1984). Subsequent northern-sourced ice advances could have remobilized such Cascades-sourced outwash and mixed it into till deposits in the Black Hills, resulting in till with a Cascades-sourced lithologic assemblage without Cascades-sourced ice ever reaching the Black Hills. We clearly observed a comparable effect in some tills near basalt-rich older substrate: tills in such settings commonly mined local basalt-rich sources and increased their basalt clast content, especially within about 2 ft of the base of the till. We therefore cannot exclude the possibility that drift with clast assemblages suggesting a Cascades source are instead tills from northern-sourced ice advances that picked up a Cascades-sourced clast mix by excavating a Cascades-sourced outwash deposit.

GLACIAL DEPOSITS

Pre-Vashon Glacial Deposits

Most pre-Vashon sediments along the eastern flank of the Black Hills lack age control, but are interpreted as glacial deposits. Northern-sourced till, outwash, and lake sediment were deposited along the eastern slope of the Black Hills during at least two southward incursions of the Cordilleran continental ice sheet into the Puget Lowland. Such incursions are thought to have occurred during even-numbered marine oxygen isotope stages (MIS).

During ice incursions into the map area, ice-dammed lakes formed in east-draining watersheds, most notably in the Waddell Creek valley. A Vashon-age "Waddell Creek Lake" was proposed by Bretz (1913). Our mapping has confirmed existence of a smaller Vashon-age lake and a larger lake during at least one pre-Vashon ice incursion (Fig. 9). We interpret moderately to heavily weathered pebbles we found scattered in clay soil as much as 800 ft in elevation within the Waddell Creek basin as dropstones from one or more pre-Vashon lake(s). This is higher than the 650 ft elevation proposed by Bretz, but consistent with his description of the deposit (albeit not the Vashon age inferred by Bretz). We assign this larger lake to a pre-Vashon age, not only based on pebble weathering, but also because we did not find any evidence that the Vashon glaciation had sufficient extent to dam a lake this high. Bretz described glaciolacustrine sediments in the lower parts of the Waddell Creek valley, which we did not definitely observe but identified as unit Qpf in our cross section on the basis of well records.

We did not find evidence supporting or negating a spillway of a pre-Vashon glacial lake Waddell into Cedar Creek, as proposed by Bretz (1913) for the Vashon ice incursion, or into Sherman Creek. We did find evidence that water drained south through the small valley at site C11, although at 690 ft elevation, this might not have been the spillway from the apex of the pre-Vashon lake, when water would have been at least 800 ft high farther north in the watershed. The deposit at site C11 is a heavily weathered, bedded pebble gravel, with no modern source for the flow of water. Multiple relict channel segments dot the eastern flank of the Black Hills south of site C11 and similarly lack a modern water source. Collectively, these suggest a partly ice-supported, southbound drainage pathway for an ice-dammed pre-Vashon lake in the Waddell Creek watershed.

During the pre-Vashon glaciation(s), small ice-dammed lakes also likely formed in the smaller east-draining valleys, such as Mill Creek and the upper Mima Creek valleys. We infer their presence but did not find deposits from these lakes and show no associated shorelines on our map. Considering the scarcity of deposits left by the larger glacial lake Waddell, it is not surprising we did not find deposits from these smaller lakes.

Vashon Glacial Deposits

Like Bretz (1913), we found evidence for a Vashon-age ice-dammed lake in the Waddell Creek basin. This lake did not rise as high as the pre-Vashon lake, but it apparently resulted in large deltaic gravel deposits, such as that at the gravel pit 2,000 ft southeast of clast count site C45 (sec. 21, T17N R3W). The delta deposits, as well as vague shoreline-like erosional features around the basin, suggest that the Vashon-age glacial lake Waddell reached about 460 ft elevation. (The "650 ft" elevation reported by Bretz as the upper limit of dropstones in the Waddell Creek basin likely included pre-Vashon stones that he interpreted as Vashon-age.) Gray clay in unit Qoa at age site GD1 (sec. 29, T17N R3W) and unit Qls at site C48 (sec. 33, T17N R3W) may be sediment from this Vashon-age lake.

Geomorphic features, including channels and small delta deposits, suggest that the Vashon-age lake drained south in a kame setting along the flank of the hills, as did Vashon periglacial drainage northeast of Waddell Creek (Fig. 9). Multiple channel systems at different elevations document how meltwater drainage pathways along the hills changed as the ice receded.

NONGLACIAL DEPOSITS

Postglacial sediment in glaciated parts of the map area can usually be distinguished from glacial sediment because it lacks the compaction that typically resulted from overriding glacial ice, but glacial overriding may be difficult to recognize in well-sorted sediment near ice margins (where ice was thin and did not exert much pressure) or where particles are well rounded and moderately or well sorted, because such deposits can be largely incompressible.

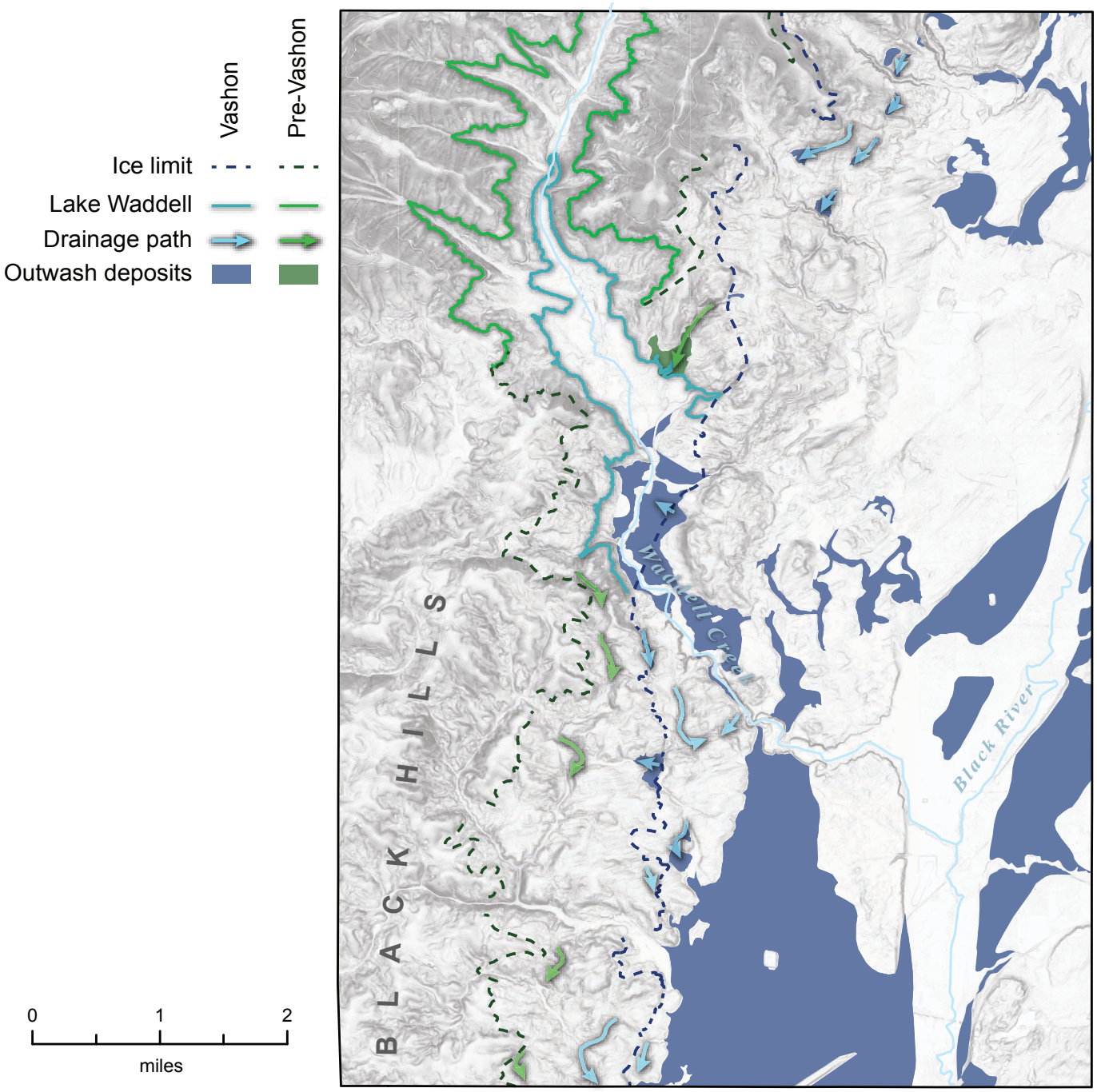

Figure 9. Vashon and pre-Vashon ice limits with corresponding lakes in the Waddell Creek valley, recessional glacial outwash deposits and periglacial drainage paths.

Postglacial deposits include both Pleistocene and Holocene deposits, because the onset of the Holocene at 11.7 ka (USGS Geologic Names Committee, 2010) does not coincide with the end of the Vashon glaciation. We estimate that Vashon ice was present in the map area between 15.8 and 15.3 ka on the basis of age-control data farther north in the Puget Lowland (fig. 3 in Polenz and others, 2015).

Because the Black Hills were never completely glaciated, there is very little constraint on the age of mass-wasting features, old alluvium, and weathering profiles. With few exceptions, our inferences of sediment age in unglaciated parts of the map area rely on stratigraphic field relations, geomorphic observations, and assessments of relative weathering (see above: *Interpretation of Weathering and MIS*). In many instances, exposures provide no indication of sediment age because there is no stratigraphic indicator of glaciations, and even historic flood-plain deposits can be pure, massive, tan to brown clay (recycled from older deposits—see also unit Qa and Bretz, 1913). This suggests that, in unglaciated areas, surficial units subject to on-going deposition (units Qa, Qaf, Qp, Qls) include some pre-Vashon sediment. It is also likely that unit Qoa does—as suggested by a radiocarbon date on wood extracted from clay at age site GD1 (sec. 29, T17N R3W; Tables M1 and A1)—although a Vashon age for that deposit is also reasonable. The radiocarbon analysis

at site GD1 suggests an age of ~17.1–16.9 ka, roughly 0.5–1.7 ky older than the arrival of the Vashon glacier (Polenz and others, 2015). However, the olive-gray clay could easily be interpreted as glaciolacustrine on the basis of its field appearance and setting. A Vashon-glacial association for this deposit cannot be excluded, because the wood sample from this analysis could have an inherited age and be several hundred years older than the deposit (Gavin, 2001).

The clay at age site GD1 may be from (1) a lake in the late pre-Vashon valley floor, (2) a Vashon ice-dammed lake with detrital wood older than the deposit, (3) a Vashon ice-dammed lake dated by an inaccurate ^{14}C analysis or inherited age, or (4) a Vashon ice-dammed lake dated accurately—in which case several radiocarbon dates farther north in the southern Puget Lowland would have to be dismissed as inaccurate (Polenz and others, 2015, 2016). We were unable to determine if the stick was detrital or part of a snag drowned in place. We mapped the deposit as unit Qoa to allow for the possibility of the deposit being either Vashon glacial or pre-Vashon nonglacial.

Mima Mounds Formation Age

Mima mounds are round to oval mounds ~2 to 6 ft high and 10 to 30 ft across; they consist of dark brown to black, organic-rich sand to pebbly sandy loam soil and rest on Vashon proglacial outwash terraces. The black color is mostly due to ash from burned organic matter. Unlike Parker and others (2005) and Logan and others (2005, 2009) in their work mostly east of the Littlerock quadrangle, we observed Mima mounds on multiple adjacent terrace levels in the Littlerock quadrangle, for instance near the southwest corner of sec. 34, T17N R3W. Mima mound fields also straddle some adjacent terraces and even occupy a gentle terrace riser near the southern map edge (secs. 10 and 15, T16N R3W), where relict channel erosion of the terrace edge above suggest that Mima mound formation on the terrace riser post-dates erosion of those channels. Some outwash terraces with Mima mounds in and near the Littlerock quadrangle are kettled, for instance at the north end of Mima Prairie, where the mounds can be found between but not inside kettles (sec. 34, T17N R3W). Barely south of the Littlerock quadrangle, apparent Mima mounds occupy gentle slopes in closed depressions that may also be kettles (sec. 15, T16N R3W). It remains unclear if these mounds formed after the depressions or were simply not noticeably disturbed by depression formation.

Sand and clast lithologies and weathering in the mounds fundamentally resemble those in the underlying outwash, although the clast assemblage in the mound matrix we examined at the Mima Mounds Natural Area (clast count at site C2, 22% intermediate igneous clasts; Fig. 10) contains slightly more Cascades-sourced clasts than the two samples of the underlying outwash (site C1, 18%, and site C3, 16% intermediate igneous clasts). All clast counts from this area (sites C1–C3) signal a less Cascades-sourced clast mix than those from unit Qgo_{y3} terraces farther east in sec. 12, T16N R3W (site C16, 24%, and site C17, 32% intermediate igneous clasts). Pringle and Goldstein (2002) suggested that the mounds are related specifically to the Tanwax Creek–Ohop Valley flood and noted that at the andesite-clast-rich Rocky Prairie (6 mi east of the Littlerock quadrangle, Fig. M1), mound matrix also contains a much larger fraction of ashy andesitic clasts.

Figure 10. Cross-sectional view of a Mima mound at clast count sites C2 and C3 in the Mima Mounds Natural Area. The mound consists of approximately 5 ft of dark brown soil above the waistline of the person on the left. Loose debris mostly obscures a sharp, planar contact and textural contrast between the mound and underlying gray, cobbly pebble gravel of Vashon recessional outwash (unit Qgog). Clast counts of 52 pebbles from the mound (site C2) and 50 clasts from unit Qgog (site C3) suggest a Cascades-sourced contribution to the clast assemblages in both deposits. Although pebbles from the mound soil appear to be slightly less weathered than clasts from the underlying outwash, the difference and sample sizes are too small to establish such a separation. Weathering is mild in both clast counts and appears to be a result of surficial soil development because the weathering distinctly exceeds clast weathering from a sample unaffected by surficial soil weathering >15 ft below the top of unit Qgog at nearby clast count site C1.

The genesis of Mima mounds is widely debated, and many hypotheses exist regarding the formation mechanism (Bretz, 1913; Washburn, 1988). The mounds are often attributed to pocket gophers—the idea being that the highly territorial burrowing rodents concentrate soil sediment in the center of their foraging area. Every time they burrow out, they push soil behind them, thus building a soil mound on top of the relatively impenetrable outwash gravel over the course of many generations (Dalquest and Scheffer, 1942; Gabet and others, 2014; Reed and Amundson, 2012; Burnham and Johnson, 2012). Other hypotheses include formation by seismic vibration (Berg, 1990) or interactions between ice, permafrost, and water (Newcomb, 1952; Richie, 1953; Logan and Walsh, 2009). We offer no new theories about their enigmatic formation.

Unit QEcf

This unit represents a subaerial weathering crust of clay soil and (or) saprolite that conceals underlying deposits. Clay thickness locally exceeds 30 ft, suggesting that weathering may have begun before the Quaternary (Greg Retallack, Univ. of Oregon, oral commun., 2016). The complete alteration of original minerals likewise indicates that the soil has been weathering for a long time, as plagioclase has been shown to have at least a 5 m.y. residence time in soil (Hausrath and others, 2008). The mineralogic and chemical characteristics of unit QEcf are further discussed below (see *Geochemistry*). Inferences of Eocene Black Hills uplift and absence of recognized post–Crescent Formation rocks, except on the margins of the Black Hills, additionally suggest that surficial exposure of Crescent Formation basalt in the Black Hills may have continued since Eocene time. Thus, the formation of the unit QEcf weathering horizon may have begun in the Eocene, and according to Livingston (1966), lateritic soils may be developing in the Pacific Northwest today.

GEOCHEMISTRY

Bedrock Unit Identification

A total of 51 samples were selected for whole rock major and trace element analysis, and these include basalts (n = 25; includes two from east of the map area), clays derived from different substrates (n = 13), and sedimentary rocks (n = 13; includes six from outside the map area; of the seven from inside the map area, four are tuffaceous siltstone or sandstone, and three are claystone).

CRESCENT FORMATION BASALT

All of the Crescent Formation samples classify as tholeiitic basalts (Figs. 11A and B) and overlap in chemical composition with previously analyzed lavas mapped as Crescent Formation (Babcock and others, 1992; Logan and Walsh, 2004; Bowman and others, 2014; Polenz and others, 2016). The Littlerock samples range from 48.7 to 50.5 wt. percent SiO_2 and have Mg-numbers (molar % Mg/Mg + Fe) between 59 and 47. On the basis of texture and chemical composition, these lavas can be divided into a more enriched group that tend to be finer-grained and found in the northern half of the map area, and a less enriched group that is coarser grained and found in the southern part of the quadrangle. The two groups are similar in their degree of differentiation (that is, they have similar ranges of SiO_2 and Mg-number), but the enriched (northern) group samples have higher TiO_2 (2.0–2.5 vs. 1.2–1.8 wt. %)(Fig. 11C) and P_2O_5, greater light rare-earth enrichment (chondrite-normalized La/Yb_N = 2.8–3.7 vs. 2.2–2.5)(Fig. 11D), higher concentrations of high-field-strength elements (for example, U, Hf, Nb, Zr), and lower Y/Nb (1.8–2.2 vs. 2.6–3.1) and Zr/Nb (10.4–11.2 vs. 11.7–12.1)(Fig. 11E). All of these differences involve elements that tends to be immobile during alteration and low-grade metamorphism, and it is therefore most likely that the chemical distinctions between the more enriched group and the less enriched group reflect contrasts in their mantle sources rather than in their magmatic differentiation or alteration histories. In general, the more enriched samples overlap compositionally with Crescent Formation lavas from the Willapa and Black Hills, while the less enriched samples overlap with data from Crescent Formation lavas of the Olympic Peninsula (Figs. 11C, D, and E).

EOCENE VOLCANIC BASALT

Basalt exposures east of the Black Hills are not part of the Crescent Frmation. Two of our basalt samples (sites G8, G19; Figs. M1 and 5) come from small exposures of Logan and others' (2009) unit Evb (site G8) and unit Eig (site G19) east of the Black Hills and Black River valley. Age site GD3 (collocated with geochemistry site G8) yielded a $^{40}Ar/^{39}Ar$ date (45.97 ±0.23 Ma). This is younger than most recently published Crescent Formation ages (56–48.4 Ma, Wells and others, 2014; Eddy and others, 2017). Samples from sites G8 and G19 differ significantly from one another in many of their chemical traits (for example, chondrite-normalized La/Yb_N = 1.4 vs. 3.2; Y/Nb = 1.7 vs. 4.2). This indicates they are not comagmatic, but both plot within the range of published Crescent Formation basalt analyses (Figs. 11C, D, and E). Rocks elsewhere in Washington that are similar in composition to Crescent Formation basalts, but younger and (or) found farther east, include middle Eocene sills mapped as unit Eig in the Willapa Hills west and southwest of the Black Hills (Moothart, 1993; Wells and others, 2014), the basalt of Summit Creek south of Mount Rainier (Kant and others, 2015), and Eocene diabase and gabbro also mapped as unit Eig in the Maytown and East Olympia quadrangles (Walsh and Logan, 2005; Logan and others, 2009). These rocks, like at sites G8 and G19, display no consistent geochemical signatures that distinguish them from Crescent Formation lavas; all were probably derived from the same mantle source(s) as the Crescent Formation, but during the waning stages of that activity.

McINTOSH FORMATION

Claystones of the McIntosh Formation in the Littlerock quadrangle are rich in nontronite, a smectite clay characteristic of a high pH environment. The clay was likely inherited or formed shortly after deposition of iron-rich fine-grained sediment (basaltic glass?) while still in the marine environment (Dixon and Weed, 1989). Although these clays could have formed in a terrestrial soil environment, we consider this less likely, mainly because the interbedded siltstones and sandstones are relatively fresh and still contain mostly intact feldspar, quartz, and some mafic mineral grains, and XRD mineral identification and petrographic analysis show moderate amounts of clay that is likely pedogenic. This

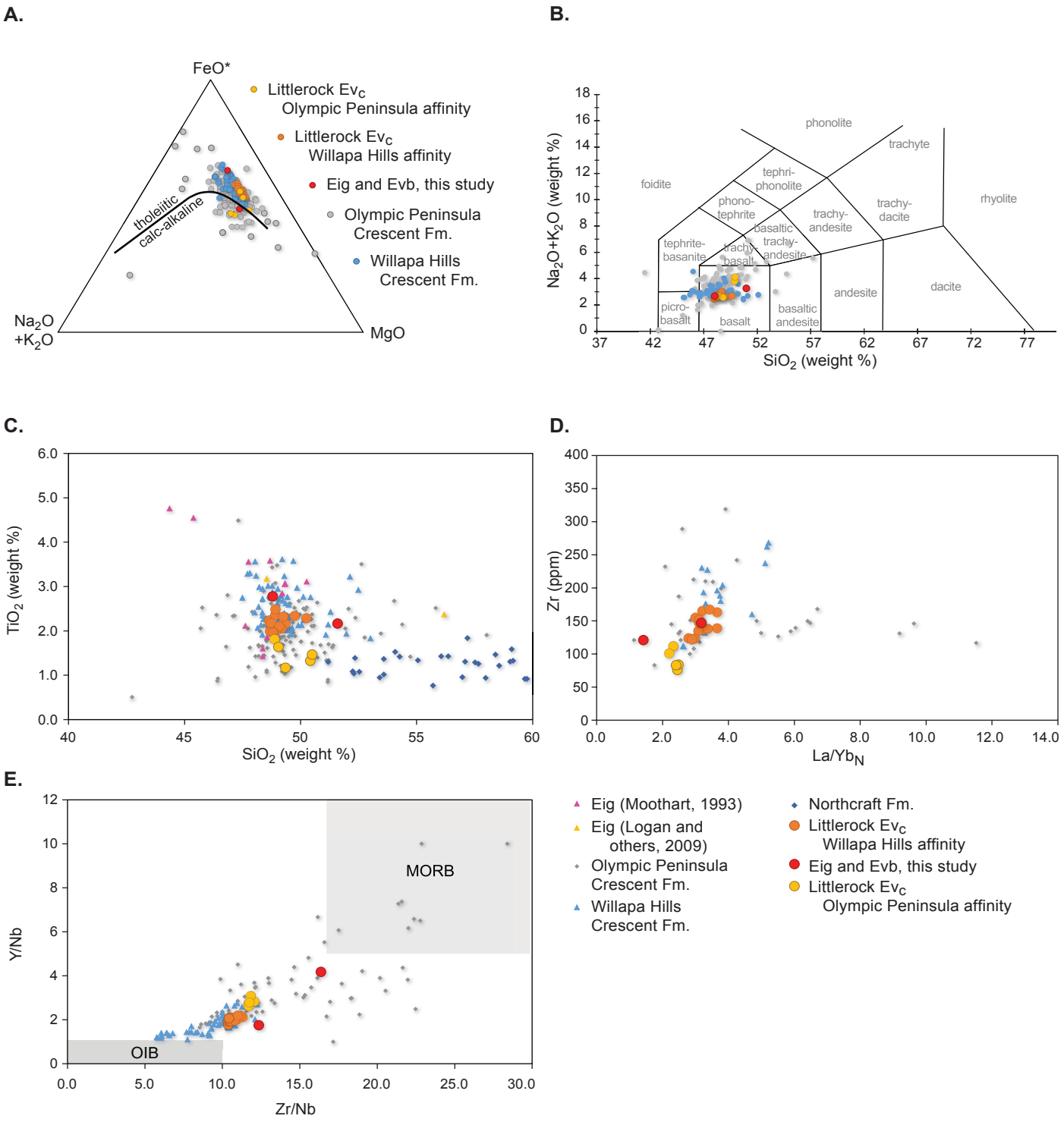

Figure 11. A. AFM diagram (Irvine and Baragar, 1971) showing that basalt samples from the Littlerock quadrangle (colored symbols) are dominantly tholeiitic and overlap in composition with analyses of Crescent Formation basalts from published literature. **B.** Total alkalis vs. silica plot (Le Bas and others, 1986) showing that Crescent Formation samples from the Littlerock quadrangle classify as subalkaline basalts and overlap in composition with Crescent Formation samples from published literature. **C.** Variation diagram comparing basalts from Littlerock quadrangle with other basalts from western Washington and volcanics of the Northcraft Formation. Note that unit Ev_C samples with Willapa Hills affinity are more enriched in TiO_2 and resemble Crescent Formation basalts from the Willapa Hills, whereas unit Ev_C samples with Olympic Peninsula affinity are less enriched and overlap data from the Olympic Peninsula. Units Evb and Eig samples from this study fall within the range of Crescent Formation data. No samples from this quadrangle show similarities to Northcraft Formation. **D.** Variation diagram comparing basalts from Littlerock quadrangle with other basalts from western Washington. Note as in previous figures that Ev_C samples with Willapa Hills affinity are more enriched (higher Zr and La/Yb_N) and resemble Crescent Formation basalts from the Willapa Hills, whereas unit Ev_C samples with Olympic Peninsula affinity are less enriched. Units Evb and Eig samples from this study again fall within the range of Crescent Formation data. **E.** Incompatible trace-element ratios of Littlerock quadrangle basalts and Crescent Formation basalts from elsewhere in Washington compared to typical values of mid-ocean-ridge basalt (MORB) and ocean-island basalt (OIB)(gray shaded areas; from LeRoux and others, 1983). Note that unit Ev_C (Willapa Hills affinity) samples plot closer to the OIB field, another indication of derivation from a more-enriched mantle source. N subscript in La/Yb ratio denotes chondrite-normalized values.

indicates that the rocks of unit Em2m in the Littlerock quadrangle are less weathered than the basalt-derived saprolite and clay soils, in which all primary minerals have been dissolved. If the McIntosh Formation claystone had been altered so completely to smectite in a terrestrial, soil-forming environment, we expect that the more porous beds of sandstone and siltstone in the same unit would likewise be heavily weathered. Also, the overlying pre-Vashon drift (site G51) is rich in halloysite and contains no nontronite. If the McIntosh Formation claystones had been weathered in an environment similar to that of the overlying drift, we would expect more-similar clay species. We infer that the abundant smectite in the McIntosh Formation did not form during terrestrial weathering of the McIntosh Formation and may be mostly inherited.

Within the McIntosh Formation, we sampled four tuffaceous sediment beds. Tuffaceous sedimentary rock at geochemistry site G23 (age site GD4, U-Pb zircon dated at 47.35 ±0.21 Ma) has the chemical attributes of adakite, indicative of derivation from an eclogitic source (that is, garnet-bearing and feldspar-poor) that is commonly interpreted as a subducted slab or deep-arc crust (Defant and Drummond, 1990; Martin and others, 2005). These affinities include Sr >400 ppm (G23 = 608 ppm), Y <18 ppm (10.4 ppm), Sr/Y >20 (58), Yb <1.8 ppm (0.9 ppm), and Al_2O_3 >15 wt. % (20.3 wt. %). Based on its chemistry (which resembles an igneous-rock composition) and petrographic character (dominated by fresh angular fragments of plagioclase and amphibole), the tuffaceous sandstone at G23 was probably reworked from an airfall tuff and likely represents a single eruptive event. Adakites of Eocene age also crop out in the Bremerton Hills (Tepper and others, 2002), the Center quadrangle (Polenz and others, 2014), and the Chimacum area (Hahn and others, 2004) and have been attributed to slab melting in response to passage of a slab window or breakoff of the Farallon slab (Kant and others, 2015). In contrast to site G23, the chemical characteristics of the other tuffaceous sediments (sites G27, G26, and G30) do not resemble igneous compositions (most notably in Al_2O_3 and K_2O contents), suggesting they contain a significant detrital component. All three have elevated Ba/Nb ratios (35 to 43), which points to a volcanic arc source.

To explore the possibility of using geochemistry to identify sedimentary rock units, major and trace element compositions were measured on two samples from each of three Tertiary formations mapped outside the Littlerock quadrangle: the Skookumchuck (sites G42 and G50), the Lincoln Creek (sites G43 and G44), and the McIntosh (sites G45 and G49). For most elements, these three formations overlap in composition, but the two McIntosh Formation samples (sites G45 and G49) have higher CaO, Na_2O, Ni, Cr, and Sr and lower Ba, Pb, Rb, Cs, and Sc (Table 1). Based on these differences, samples from sites G36 and G37 (unit Em2m inside the Littlerock quadrangle) are more similar to the Skookumchuck or Lincoln Creek Formations than the two McIntosh Formation samples from outside the Littlerock quadrangle (sites G45 and G49). This suggests that these formations are too close in composition to be distinguished chemically on the basis of the small number of available analyses, but it is possible that, with additional samples, these formations may be discernible.

Clay Mineralogy, Chemistry, and Weathering

Fourteen clay samples (units QEcf and Qpd) were analyzed to assess whether chemical data might be useful in future mapping studies for inferring parent material, and if so, which elements would be most useful. Comparison of data for six clay samples derived from weathering of basalt and six derived from weathering of glacial drift reveals clear differences, with clays developed from basalt being higher in TiO_2, Al_2O_3, FeOt[3], and P_2O_5, and clays developed on drift being higher in SiO_2, CaO, Na_2O, and K_2O (Table 1; Figs. 12a,b). In general, major elements appear to be better than trace elements for discriminating between basalt- and drift-derived clays, although Sr, Sc, and Ni also serve this purpose.

Although differences in major element compositions can be used to differentiate basalt-derived clays from drift-derived clays, these differences can also be affected by weathering. TiO_2, Al_2O_3, FeOt, and P_2O_5 are all relatively immobile during soil weathering and will be concentrated, while SiO_2, CaO, Na_2O, and K_2O are more mobile and are progressively leached out as soil weathering progresses (Eggleton and others, 1987). Thus, a less-weathered basalt soil or an older drift-derived soil might be mistakenly identified using these metrics.

The mineralogies of the basalt- and drift-derived clays share some traits, with halloysite and goethite being the dominant clay species in both groups. Both of these minerals are commonly

[3] Total iron oxides regardless of oxidation state.

Table 1. Comparison of normalized chemical compositions of clays derived from basalt and drift (major elements in wt. %, trace elements in ppm). These twelve elements provide the best discrimination. Values are averages (n=6) reported with standard deviation. Analyses of two outliers, sites G31 and G38, were excluded from the comparison—see text and unit descriptions for units QEcf (G31) and Qpd (G38).

	SiO_2 (wt. %)	TiO_2 (wt. %)	Al_2O_3 (wt. %)	FeOt (wt. %)	MgO (wt. %)	CaO (wt. %)	Na_2O (wt. %)	K_2O (wt. %)	P_2O_5 (wt. %)	Sr (ppm)	Sc (ppm	Ni (ppm)
Basalt (unit QEcf)	40	4.6	30	24	1.1	0.1	0.1	0.2	0.4	27	58	109
	(5.7)	(1.8)	(2.7)	(6.1)	(0.5)	(0.1)	(0.04)	(0.17)	(0.15)	(18)	(11)	(20)
Drift (unit Qpd)	60	2	22	11	1.7	0.9	1.1	0.9	0.2	99	28	69
	(5.2)	(0.6)	(3)	(2.6)	(0.3)	(0.23)	(0.4)	(0.31)	(0.04)	(34)	(11)	(15)

formed in terrestrial soils, but halloysite needs an acidic, leaching environment to form (Dixon and Weed, 1989). This is in contrast to the previously discussed nontronite clay in the McIntosh Formation, which requires a basic, non-leaching environment to form and persist. As to the other constituents, the drift-derived clays retained varied but significant amounts of quartz, feldspar, and some mafic minerals, whereas the basalt-derived clays contained little or none of their original minerals (Table DS9).

According to Hausrath and others (2008), plagioclase has a 5 m.y. persistence time in soil, and Colman (1982) reported that the complete destruction of the primary minerals in basalt and andesite takes at least several hundred thousand years in the western U.S. The absence of primary minerals in the Crescent-derived saprolites and soils and the tremendous thickness of the soils (30+ ft) support the inference that basalt surfaces in the Black Hills have been subaerially exposed since well before the Quaternary, and definitely longer than the pre-Vashon drift along the eastern flank of the Black Hills. The inference of extended basalt weathering is reinforced by the presence of outcrops, such as in Figure 2, where less-weathered clay from pre-Vashon drift rests on more-weathered, basalt-derived clay, suggesting that the basalt was already significantly weathered when the (then fresh) drift was deposited.

Site G32 (sec. 8, T16N R3W) yielded the basalt-derived clay sample with the highest halloysite content and the only basalt-derived sample that also contains kaolinite, an indicator of advanced weathering (Joussein and others, 2005). We collected a sample at site G32 from a patch of unit QEcf that was surrounded by unit Em2m. We field-interpreted this patch as basalt-derived. Soil in the surrounding unit Em2m is less weathered, and still contains some of its original minerals. Although we were unable to observe contact relations that definitively place unit Em2m in this area atop the Crescent Formation basalt that we believe underlies the area, we suggest that the patch of unit QEcf at site G32 is a basalt mound that pokes up through the surrounding drape of unit Em2m, and that the more advanced weathering in the basalt began before the surrounding McIntosh Formation was deposited. We were unable to confirm this with the available data, but our inability to disprove it contributed to our decision to map the largely basalt-derived unit QEcf as weathering product that may have begun to form during the Eocene.

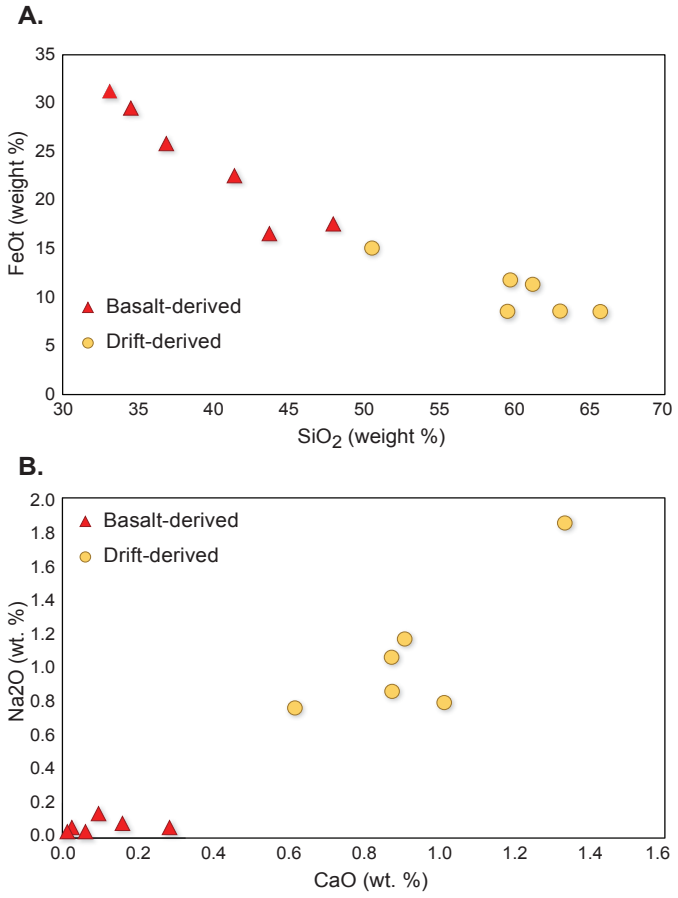

Figure 12. Compositions of clays derived from basalt compared to clays derived from drift. **A.** FeOt vs. SiO_2. **B.** Na_2O vs. CaO.

To explore the formation of the clay-rich saprolite and soils, we sampled weathering profiles where we were fairly sure of the parent materials and compared the saprolite/soil chemistry to the parent material (Figs. 2 and 4). We found that overall, soil-weathering principles were upheld, with more-weathered samples depleted of SiO_2, CaO, and K_2O and enriched in Fe_2O_3, Al_2O_3, and TiO_2. At site G48 (Fig. 4), we sampled core-stones, saprolite, and soil. We found that the saprolite and soil are similar in composition. Both contain much more Fe_2O_3 and Al_2O_3 than the core-stone. At site G47 (Fig. 2), the same pattern was recognized from core-stones to saprolite. The drift below the soil, though basalt-rich, showed less weathering in both the mineral content and bulk geochemistry, with some original minerals still present, more SiO_2 than the saprolite, and less concentration of Fe_2O_3. At sites G29 and G34, the apparently basalt-derived soils retained some mineralogic quartz that was identified in the XRD analysis. Site G29 also had 40 wt. percent SiO_2, one of the highest sampled. This sample was collected well above the elevation of recognized glacial incursions, so the quartz content may represent the addition of loess.

Placer Gold

Oral history reports of at least one historic gold mining camp (Inez Bond, private landowner, oral commun., 2016) and the persistent popularity of recreational gold panning in Capitol State Forest motivated sampling of stream sediment at five locations to assess gold content and explore possible gold sources. At each site, the medium sand and finer particles from a bulk sample and a panned sample were separately analyzed (see *Methods*). Six samples from three sites (G54–G59, Fig. 5) targeted sub-basins of Waddell Creek. Two samples from one site (G52–G53, Fig. 5) targeted glacial sediment with little or no expected contribution from local bedrock. The fifth site, located 2.1 mi west of the Littlerock quadrangle along South Fork Porter Creek (sites G60–G61, Fig. M1), targeted a watershed mapped entirely as Crescent Formation basalt (Logan, 1987; Walsh and others, 1987), with no expected or observed contribution to the stream bedload of either sedimentary rocks or glacial sediment.

The analytical results are presented in Table DS11. Six of the ten analyses yielded no detectable gold. Of those, four were panned (sites G53, G55, G57, and G61), and two were bulk stream bedload (sites G54 and G58). Two stream bedload bulk samples (sites G56 and G60) and one panned sample (site G59) each yielded 0.001 ppm gold content—barely enough for

detection. One bulk sample (site G52) yielded 1.115 ppm gold content—a concentration that exceeds what many successful commercial mines recover from ore (Richard Goldfarb, USGS retired, written commun., 2017).

These results suggest that panning did not concentrate gold in our samples. Possible explanations include that (1) the gold is concentrated in very fine particles that are readily washed out during panning, despite their high specific gravity; (2) the gold is concentrated in mineral grains or rock fragments whose specific gravity is too low to be effectively concentrated during panning; (3) the gold is concentrated in mineral grains or rock fragments larger than medium sand (and was therefore excluded from the analysis); and (4) we are poor panners. Successful recreational panners in the Black Hills typically end up with very fine gold particles, suggesting that the gold is generally concentrated in small flecks, many of which may have been flushed out during our panning.

The minimal gold content in all samples from Waddell Creek and South Fork Porter Creek, all of which likely derive most of their sediment from Crescent Formation basalt in the Black Hills, suggests that these basaltic rocks contain little gold. If the Crescent Formation were to yield appreciable gold, it would most likely be from sedimentary rocks, which, if metamorphosed to at least lowest greenschist facies (as might have occurred during accretion of Siletzia), would contain quartz-carbonate veins with grains of gold. Such veins might be small, widely scattered, and uneconomic, but one would expect some resulting gold grains in streams to be coarse, and scheelite, arsenopyrite, or cinnabar might be present as associated minerals (Richard Goldfarb, written commun., 2017). There is no indication that the headwaters of our sample sites include significant sedimentary rocks, and the only sample that yielded enough gold to suggest possible presence of a coarser gold grain was at site G52, the bulk sample from the one site specifically selected to target glacial deposits. This suggests that the best source for gold in the Black Hills is glacial deposits, not Black Hills bedrock. An alternative interpretation is that a fairly rich source of gold is present upstream of site G52. If so, it would require the presence there of some bedrock not presently recognized in this part of the Littlerock quadrangle, most likely sedimentary rock metamorphosed at moderate temperatures to at least low greenschist facies.

STRUCTURES IN THE MAP AREA

The Black Hills are marked by numerous prominent topographic and geophysical lineaments, some of which approximate orientations of faults mapped outside the Littlerock quadrangle. These lineaments suggest that faults mapped outside the Littlerock quadrangle extend into it. However, where lineaments extend into the map area, the thick clay soil or glacial deposits obscure any potential surface evidence of faulting. Like Logan and Walsh (2004) north of our map area, we observed columnar joint orientations to be varied and generally not useful for assessment of flow orientations.

West of the Littlerock quadrangle (0.9 mi), at a 10 to 13 ft high basalt bedrock knickpoint, a cluster of near-vertical joints and possibly shears strike roughly east–west in basalt bedrock along a stream channel. These features are located along a strong east–west lineament 0.8 mi south of Capitol Peak (significant sites S4 and S5, Fig. M1). Within the Littlerock quadrangle 1.5 mi east-northeast of sites S4 and S5, the strike and dip of a 5 cm (~2 in.) thick shear in weathered basalt was measured at 091/78—closely resembling the orientation of the joints along the lineament.

A freshly blasted quarry wall at geochemical site G5 (sec. 8, T16N R3W) revealed a 50 ft high exposure of a prominent and well-exposed, approximately vertical fault striking 120° across a single(?) basalt flow (Fig. 13). The 6 ft wide sheared zone includes two main shears with gouge as much as 50 cm (~20 in.) thick. The character of the basalt on one side of the fault resembles that on the other. Rakes on slickensides dip steeply southeast; up-direction is unclear. Farther northwest (0.8 mi), the active channel of Mill Creek (sec. 6, T16N R3W) revealed a shear, or less likely a vein, striking 325°, dipping 55 degrees NE, and 1 cm (0.4 in.) thick with apparent breccia fill. Both sides are flanked by basalt. On the north side of the channel is a 5 cm (~2 in.) wide zone with shear-parallel jointing. Near our two shear measurements, several joints along Mill Creek, Mima Creek, and about 2.5 mi farther north along Waddell Creek revealed similar northwest strikes. No prominent topographic or aeromagnetic lineament marks these exposures.

Aeromagnetic anomalies abound elsewhere within the Littlerock quadrangle (Fig. 5). A particularly prominent, northwest-trending, linear, southwest-down anomaly enters the map area at the southeast map corner. It is also clearly defined by ground-based magnetic survey data (magnetic data collection lines 1 and 2, secs. 3 and 10, T16N R3W, and secs. 2, 11, and 14, T16N R3W, respectively; see map sheet). Seismic depth-to-bedrock estimates at sites GP1–GP6 near this anomaly (map sheet)suggest a corresponding southwest-down lowering of the bedrock surface beneath a few hundred feet of sediment—seismic data collection points GP1 to GP4 (sec. 35, T17N R3W, and secs. 1, 2, and 12, T16N R3W) suggest shallow bedrock between –65 and +65 ft elevation northeast of the magnetic anomaly. Southwest of the anomaly, seismic measurements at sites GP5 and GP6 (secs. 3 and 10, T16N R3W) suggest a bedrock surface elevation between –270 ft and –130 ft along the northeastern margin of a magnetic trough that we informally refer to as the Mima Prairie basin (Fig. M2). Sites GP5 and GP6 are not centered in the basin, signaling that bedrock may be even lower elsewhere in the basin. Well no. 22 (map plate, W22) is located slightly west of the basin and shows basalt bedrock 230 ft below the surface, or 14 ft below sea level, consistent with the bedrock surface rise interpreted from the aeromagnetic anomaly map. We therefore infer that the Mima Prairie basin is a bedrock depression southwest of a strong, straight, northwest-trending magnetic anomaly beneath Mima Prairie and the lower Black River valley (near the southeast end of the quadrangle; Fig. M2).

Structural Interpretation and Tectonic Context

Before concluding that the Mima Prairie basin is structural, we explored if it might be a product of fluvial erosion because meltwater from incursions of Cordilleran ice could scour a deep valley in or near the Black River and Chehalis valleys. However,

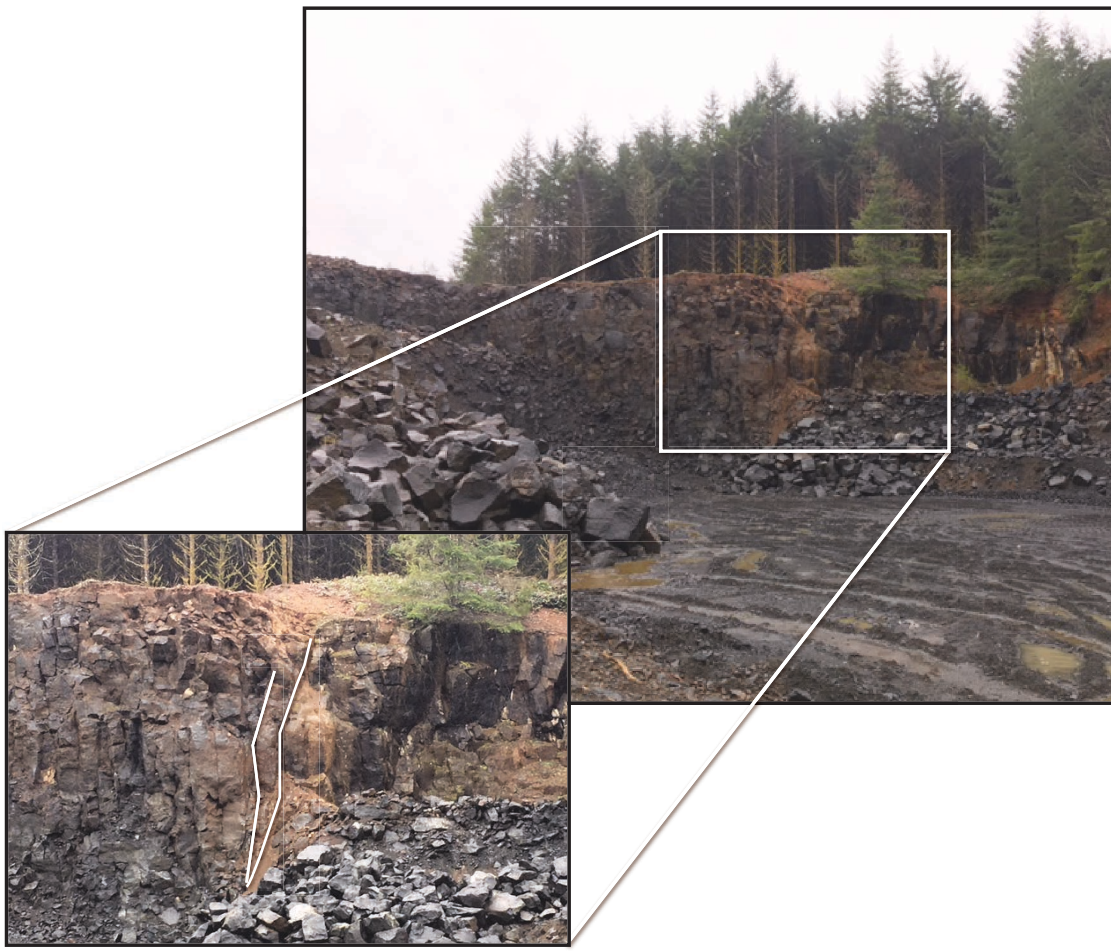

Figure 13. Fault exposed in an east-facing quarry wall. Fault strikes 120° and is nearly vertical.

the geophysical data do not suggest a channel-like bedrock trough across or near the Mima Prairie basin.

The 120° and 325° strikes of shears within the Littlerock quadrangle approximate the orientations of the Scammon Creek, Kopiah, Newaukum, and Coal Creek faults, as well as several unnamed faults and fault-parallel folds mapped south and southeast of the Littlerock quadrangle (Snavely and others, 1958; WGS, 2016b)(Fig. M1). Northwest-striking aeromagnetic lineaments and anomalies are similarly oriented along those faults and across much of the Littlerock quadrangle, including the northeast and southwest bounds of the Mima Prairie basin (Fig. M2). Straight stream reaches and other topographic lineaments with similar, northwest-trending alignments are also readily apparent within and outside the Littlerock quadrangle. We conclude that the Mima Prairie basin and associated aeromagnetic anomalies likely are expressions of structures related to the northwest-striking, mostly northeast-up cluster of faults mapped by Snavely and others (1958). We therefore tentatively infer a concealed, northeast-up, northwest-striking fault along the northeast margin of the Mima Prairie basin (Fig. M2) and suggest that it may be a northwest extension of Snavely and others' (1958) Coal Creek fault, Newaukum fault, or a related fault. The two faults we observed at geochemical sample site G5 and along Mill Creek 0.8 mi northwest of site G5 may also be part of Snavely and others' northwest-striking fault cluster, but we do not infer them beyond our observation sites because we see no evidence that either marks contrasting bedrock types, significant vertical bedrock offset, or a coincidence with adjacent magnetic or topographic lineaments.

West-striking joints similarly coincide with nearby topographic and aeromagnetic lineaments and thereby invite speculation that they also align with structures in the map area and beyond. The west-trending lineament and collocated bedrock channel knickpoints at significant sites S4 and S5 west of the Littlerock quadrangle (Fig. M1) may be related to an unnamed fault mapped farther west by Pease and Hoover (1957). This lineament becomes much less defined within the map area, and we were unable to map a corresponding fault. However, we noted a west-striking shear in the map area slightly farther north (sec. 7, T17N R3W), and the observation of bedrock structures coincident with the topographic lineaments at significant sites S4 and S5 suggests that the major lineaments and aeromagnetic anomalies within and near the Littlerock quadrangle are structurally controlled. This inference is consistent with Globerman's (1981) observation of varied paleomagnetic rotation angles in Black Hills basalt, and his assertion that the Black Hills are cut by normal and reverse faults (that he did not map).

The mapped faults, measured joints and shears, aeromagnetic anomalies and lineaments, and topographic lineaments within and near the Littlerock quadrangle seem to form a cluster of features whose orientations resemble the pattern of active crustal faults farther north in the Puget Lowland. Most of the features broadly trend northwest, several trend west, and a few trend northeast. Like the Southern Whidbey Island fault zone, the Scammon Creek, Kopiah, Newaukum, and Coal

Creek faults and several unnamed faults at similar orientations form a prominent northwest-striking cluster of faults. Like the Seattle Fault apparently splaying west away from the Southern Whidbey Island fault zone, the Doty fault seems to splay west away from the Coal Creek fault. And like the Seattle Fault, the Doty fault seems to mark the southern terminus of several northwest-striking faults. Taken together, these features in and near the Littlerock quadrangle appear to be fully compatible with the kind of actively north–south compressional setting recognized farther north in the Puget Lowland—with a cluster of prominent northwest trends, common east–west trends, several northeast trends, and a few strays at varied orientations. Although we observed some joints and shears at suitable orientations, we have no field data to indicate that these features are faults, much less active faults, but we note that a north–south compressional setting is consistent with regional crustal motions and should be expressed in many, perhaps even most, of the above-noted features being active faults. However, in contrast to the Seattle and Southern Whidbey Island fault zones, the Black Hills and the area to the southeast lack a notable record of recorded crustal seismic activity.

ACKNOWLEDGMENTS

This geologic map was funded in part by the USGS National Cooperative Geologic Mapping Program under award no. G16AC00286. We thank: Ken Clark (Univ. of Puget Sound) for a field review and assistance with interpretation of bedrock; Dan Miggins (Oregon State Univ.) for $^{40}Ar/^{39}Ar$ analysis; Elizabeth Nesbitt (Burke Museum) for analysis of biostratigraphic samples for fossils and their ages; Richard Goldfarb (USGS retired) for assistance with gold-related placer sampling strategy, analytical methods, and interpretation; Wendy Gerstel for advice, coaching, and assistance with placer sampling and panning; Richard Blakely (USGS) for aeromagnetic anomaly maps; Washington DNR Natural Heritage staff Joe Arnett, Tynan Gramm-Ramm-Granberg, and Joe Rocchio for assistance with identification and paleoenvironmental interpretation of plant samples; Matt Granitto (USGS) for assistance with USGS geochemical databases; Greg Retallack (Univ. of Oregon) for advice on sampling, analysis and interpretation of clay-rich soils; WGS staff Dave Burris, Ian Hubert, Daniel Eungard, Ashley Cabbibo, Abigail Gleason, and Guy McWethy, for help with field work; Todd Lau, Spenser Scott, and Alex Kover for geophysical field data collection and analysis; Trevor Contreras and Kara Jacobacci for lidar- and field-based reconnaissance assessment of some potentially unstable slopes; Dylan Chase for assistance with well log analysis; Daniel Eungard for help with field work and geochemical analysis; Timothy Walsh, Mitchell Allen, and Alex Steely for helpful discussions. We thank private and public landowners for sharing local knowledge and permitting us to map on their land. Among coauthors, Jeff Tepper focused on geochemical analysis and interpretation; Recep Cakir on geophysical data collection and analysis; Gabriel Legorreta Paulín on satellite data; and Shannon Mahan on luminescence sample processing, analysis, and Quaternary stratigraphic interpretation.

REFERENCES

Armentrout, J. M.; Hull, D. A.; Beaulieu, J. D.; Rau, W. W., 1983, Correlation of Cenozoic stratigraphic units of western Oregon and Washington: Oregon Department of Geology and Mineral Industries Oil and Gas Investigation 7, 90 p., 1 plate. [http://www.oregongeology.org/pubs/ogi/OGI-07.pdf]

Babcock, R. S.; Burmester, R. F.; Engebretson, D. C.; Warnock, A. C.; Clark, K. P., 1992, A rifted margin origin for the Crescent basalts and related rocks in the northern Coast Range volcanic province, Washington and British Columbia: Journal of Geophysical Research, v. 97, no. B5, p. 6799-6821. [http://cedar.wwu.edu/geology_facpubs/31/]

Babcock, R. S.; Suczek, C. A.; Engebretson, D. C., 1994, The Crescent "terrane", Olympic Peninsula and southern Vancouver Island. *In* Lasmanis, Raymond; Cheney, E. S., convenors, Regional geology of Washington State: Washington Division of Geology and Earth Resources Bulletin 80, p. 141-157. [http://www.dnr.wa.gov/publications/ger_b80_regional_geol_wa_2.pdf]

Ballantyne, C. K., 2002, Paraglacial geomorphology: Quaternary Science Reviews, v. 21, no. 18-19, p. 1935-2017.

Berg, A. W., 1990, Comment and reply on "Formation of Mima mounds—A seismic hypothesis"; Reply: Geology, v. 18, no. 12, p. 1260-1261.

Blakely, R. J.; Sherrod, B. L.; Wells, R. E.; Weaver, C. S.; McCormack, D. H.; Troost, K. G.; Haugerud, R. A., 2004, The Cottage Lake aeromagnetic lineament—A possible onshore extension of the southern Whidbey Island fault, Washington: U.S. Geological Survey Open-File Report 2004-1204, 60 p. [http://pubs.er.usgs.gov/publication/ofr20041204]

Booth, D. B.; Troost, K. G.; Clague, J. J.; Waitt, R. B., 2004, The Cordilleran ice sheet. *In* Gillespie, A. R.; Porter, S. C.; Atwater, B. F., editors, The Quaternary period in the United States: Elsevier, p. 17-43.

Bowman, J. D.; Czajkowski, J. L., 2016, Washington State seismogenic features database—GIS data: Washington Division of Geology and Earth Resources Digital Data Series 1, version 4.1, originally issued December 2013.

Bowman, J. D.; Czajkowski, J. L.; Reidel, S. P.; Boschmann, D. E.; Fusso, L. A., 2014, Washington State rock geochemistry database—GIS data: Washington Division of Geology and Earth Resources Digital Data Series 5, version 1.0. [http://www.dnr.wa.gov/publications/ger_portal_geochemistry.zip]

Bretz, J H., 1913, Glaciation of the Puget Sound region: Washington Geological Survey Bulletin 8, 244 p., 3 plates. [http://www.dnr.wa.gov/publications/ger_b8_glaciation_pugetsound.pdf]

Burnham, J. L. H.; Johnson, D. L., editors, 2012, Mima Mounds—The case for polygenesis and bioturbation: Geological Society of America Special Paper 490, 205 p.

Carson, R. J., 1970, Quaternary geology of the south-central Olympic Peninsula, Washington: University of Washington Doctor of Philosophy thesis, 67 p., 4 plates.

Carson, R. J., 1980, Quaternary, environmental, and economic geology of the eastern Olympic Peninsula, Washington: [unpublished], 275 p.

Clowes, R. M.; Brandon, M. T.; Green, A. G.; Yorath, C. J.; Sutherland Brown, A.; Kanasewich, E. R.; Spencer, C. J., 1987, LITHOPROBE—Southern Vancouver Island—Cenozoic subduction complex imaged by deep seismic reflections: Canadian Journal of Earth Sciences, v. 24, no. 1, p. 31-51.

Colman, S. M., 1982, Chemical weathering of basalts and andesites—Evidence from weathering rinds: U.S. Geological Survey Professional Paper 1246, 51 p. [https://pubs.er.usgs.gov/publication/pp1246]

Colman, S. M.; Pierce, K. L., 1981, Weathering rinds on andesitic and basaltic stones as a Quaternary age indicator, western United States: U.S. Geological Survey Professional Paper 1210, 56 p. [https://pubs.er.usgs.gov/publication/pp1210]

Crandell, D. R.; Mullineaux, D. R.; Waldron, H. H., 1958, Pleistocene sequence in southeastern part of the Puget Sound lowland, Washington: American Journal of Science, v. 256, no. 6, p. 384-397.

Czajkowski, J. L., 2016, Washington State geochronology database—GIS data: Washington Division of Geology and Earth Resources Digital Data Series 6, version 1.1, originally released November, 2014. [http://www.dnr.wa.gov/publications/ger_portal_geochronology.zip]

Dalquest, W. W.; Scheffer, V. B., 1942, The origin of the Mima mounds of western Washington: Journal of Geology, v. 50, no. 1, p. 68-84.

Defant, M. J.; Drummond, M. S., 1990, Derivation of some modern arc magmas by melting of young subducted lithosphere: Nature, v. 347, p. 662-665, doi:10.1038/347662a0.

Dixon, J. B.; Weed, S. B., editors, 1989, Minerals in soil environments; 2nd ed.: Soil Science Society of America Book Series 1, 1244 p.

Dragovich, J. D.; Gilbertson, L. A.; Lingley, W. S., Jr.; Polenz, Michael; Glenn, Jennifer, 2002, Geologic map of the Fortson 7.5-minute quadrangle, Skagit and Snohomish Counties, Washington: Washington Division of Geology and Earth Resources Open File Report 2002-6, 1 sheet, scale 1:24,000. [http://www.dnr.wa.gov/publications/ger_ofr2002-6_geol_map_fortson_24k.pdf]

Duncan, R. A., 1982, A captured island chain in the coast range of Oregon and Washington: Journal of Geophysical Research, v. 87, no. B13, p. 10,827-10,837.

Eddy, M. P.; Clark, K. P; Polenz, Michael, 2017, Age and volcanic stratigraphy of the Eocene Siletzia oceanic plateau in Washington and Vancouver Island: Lithosphere, L650.1, first published on May 25, 2017, doi:10.1130/L650.1.

Eggleton, R. A.; Foudoulis, C.; Varkevisser, D., 1987, Weathering of basalt—Changes in rock chemistry and mineralogy: Clays and Clay Minerals, v. 35, no. 3, p. 161-169.

Erdmann, C. E.; Bateman, A. F., Jr., 1951, Geology of dam sites in southwestern Washington; Part II—Miscellaneous dam sites on the Cowlitz River above Castle Rock, and the Tilton River, Washington: U.S. Geological Survey Open-File Report 51-27, 314 p., 18 plates. [https://pubs.er.usgs.gov/publication/ofr5127]

Gabet, E. J.; Perron, J. T.; Johnson, D. L., 2014, Biotic origin for Mima mounds supported by numerical modeling: Geomorphology, v. 206, p. 58-66.

Gao, Haiying; Humphreys, E. D.; Yao, Huajian; van der Hilst, R. D., 2011, Crust and lithosphere structure of the northwestern U.S. with ambient noise tomography—Terrane accretion and Cascade arc development: Earth and Planetary Science Letters, v. 304, p. 202-211.

Gavin, D. G., 2001, Estimation of inbuilt age in radiocarbon ages of soil charcoal for fire history estimation: Radiocarbon, v. 43, no. 1, p. 27-44.

Glassley, W. E., 1974, Geochemistry and tectonics of the Crescent volcanic rocks, Olympic Peninsula, Washington: Geological Society of America Bulletin, v. 85, no. 5, p. 785-794.

Globerman, B. R., 1981, Geology, petrology, and paleomagnetism of Eocene basalts from the Black Hills, Washington coast range: Western Washington University Master of Science thesis, 373 p., 1 plate.

Globerman, B. R.; Beck, M. E., Jr.; Duncan, R. A., 1982, Paleomagnetism and tectonic significance of Eocene basalts from the Black Hills, Washington coast range: Geological Society of America Bulletin, v. 93, no. 11, p. 1151-1159.

Groome, W. G.; Thorkelson, D. J.; Friedman, R. M.; Mortensen, J. K.; Massey, N. W. D.; Marshall, D. D.; Layer, P. W., 2003, Magmatic and tectonic history of the Leech River Complex, Vancouver Island, British Columbia—Evidence for ridge-trench intersection and accretion of the Crescent Terrane. *In* Sisson, V. B.; Roeske, S. M.; Pavlis, T. L., editors, Geology of a transpressional orogen developed during ridge-trench interaction along the North Pacific margin: Geological Society of America Special Paper 371, p. 327-353. [http://www.sfu.ca/~dthorkel/linked/groome%20et%20al%20leech%20river%20gsa%20spec%20pap%20371%2003.pdf]

Hahn, M.; Graettinger, A.; Gustafson, J.; Ponzini, C.; Wolfe, M.; Peters, R.; Stein, K.; Tepper, J., 2004, Eocene pyroclastic deposits at Chimacum, Washington—Adakite magmetism in the Cascadia forearc [abstract]: Geological Society of America Abstracts with Programs, v. 36, no. 4, p. 69.

Haugerud, R. A., 2009, Preliminary geomorphic map of the Kitsap Peninsula, Washington: U.S. Geological Survey, Open-File Report 2009-1033, 2 sheets, scale 1:36,000 [http://pubs.usgs.gov/of/2009/1033/]

Hausrath, E. M.; Navarre-Sitchler, A. K.; Sak, P. B.; Steefel, C. I.; Brantley, S. L., 2008, Basalt weathering rates on Earth and the duration of liquid water on the plains of Gusev Crater, Mars: Geology, v. 36, no. 1, p. 67-70.

Irving, E., 1979, Paleopoles and paleolatitudes of North America and speculations about displaced terrains: Canadian Journal of Earth Sciences, v. 16, no. 3, p. 669-694.

Irvine, T. N.; Baragar, W. R. A., 1971, A guide to the chemical classification of the common volcanic rocks: Canadian Journal of Earth Sciences, v. 8, no. 5, p. 523-548.

Jackson, S. E.; Pearson, N. J.; Griffin, W. L.; Belousova, E. A., 2004, The application of laser ablation-inductively coupled plasma-mass spectrometry to in situ U-Pb zircon geochronology: Chemical Geology, v. 211, p. 47-69.

Jeschke, D. A.; Eungard, D. W.; Troost, K. G.; Wisher, A. P., 2016, Subsurface database of Washington State—GIS data: Washington Division of Geology and Earth Resources Digital Data Series 11, version 1.2, previously released October 2015. [http://www.dnr.wa.gov/publications/ger_portal_subsurface_database.zip]

Johnson, S. Y.; Blakely, R. J.; Stephenson, W. J.; Dadisman, S. V.; Fisher, M. A., 2004, Active shortening of the Cascadia forearc and implications for seismic hazards of the Puget Lowland: Tectonics, v. 23, TC1011, doi:10.1029/2003TC001507, 2004, 27 p.

Johnson, S. Y.; Potter, C. J.; Armentrout, J. M.; Miller, J. J.; Finn, C. A.; Weaver, C. S., 1996, The southern Whidbey Island fault—An active structure in the Puget Lowland, Washington: Geological Society of America Bulletin, v. 108, no. 3, p. 334-354, 1 plate.

Johnston, S. T.; Acton, Shannon, 2003, The Eocene southern Vancouver Island orocline—A response to seamount accretion and the cause of fold-and-thrust belt and extensional basin formation: Tectonophysics, v. 365, p. 165–183, doi:10.1016/S0040-1951(03)00021-0. [http://web.uvic.ca/~stj/Assets/PDFs/03%20STJ%20%26%20SA%20tecto.pdf]

Joussein, E.; Petit, S.; Churchman, J.; Theng, B.; Righi, D.; Delvaux, B., 2005, Halloysite clay minerals—A review: Clay minerals, v. 40, no. 4, p. 383-426.

Kant, L. B.; Tepper, J. H.; Eddy, M. P., 2015, Basalt of Summit Creek—Eocene magmatism associated with Farallon slab break off [abstract V^{23}C-03]: [presented at 2015 Fall Meeting] American Geophysical Union, San Francisco, Calif., 14-18 Dec.

Klepeis, K. A.; Crawford, M. A.; Gehrels, George, 1998, Structural history of the crustal-scale Coast shear zone north of Portland Canal, southeast Alaska and British Columbia: Journal of Structural Geology, v. 20, no. 7, p. 883-904.

Kuiper, K. F.; Deino, A.; Hilgen, F. J.; Krijgsman, W.; Renne, P. R.; Wijbrans, J. R., 2008, Synchronizing rock clocks of Earth history: Science, v. 320, no. 5875, p. 500-504.

Le Bas, M. J.; Le Maitre, R. W.; Streckeisen, A. L.; Zanettin, Bruno, 1986, A chemical classification of volcanic rocks based on the total alkali-silica diagram: Journal of Petrology, v. 27, part 3, p. 745-750.

Lea, P. D., 1984, Pleistocene glaciation at the southern margin of the Puget lobe, western Washington: University of Washington Master of Science thesis, 96 p., 3 plates.

LeRoux, A. P.; Dick, H. J. B.; Erlank, A. J.; Reid, A. M.; Frey, F. A.; Hart, S. R., 1983, Geochemistry, mineralogy, and petrogenesis of lavas erupted along the southwest Indian Ridge between the Bouvet triple junction and 11 degrees east: Journal of Petrology, v. 24, p. 267–318.

Lewis, J. C.; Unruh, J. R.; Twiss, R. J., 2003, Seismogenic strain and motion of the Oregon coast block: Geology, v. 31, no. 2, p. 183-186.

Lisiecki, L. E.; Raymo, M. E., 2005, A Pliocene-Pleistocene stack of 57 globally distributed benthic $\delta^{18}O$ records: Paleoceanography, v. 20, 17 p., PA1003, doi:10.1029/2004PA001071.

Livingston, V. E., Jr., 1966, Geology and mineral resources of the Kelso–Cathlamet area, Cowlitz and Wahkiakum Counties, Washington: Washington Division of Mines and Geology Bulletin 54, 110 p., 2 plates, scale 1:24,000. [http://www.dnr.wa.gov/publications/ger_b54_geol_min_res_kelso_cathlemet.pdf]

Logan, R. L., compiler, 1987, Geologic map of the Chehalis River and Westport quadrangles, Washington: Washington Division of Geology and Earth Resources Open File Report 87-8, 16 p., 1 plate, scale 1:100,000. [http://www.dnr.wa.gov/publications/ger_ofr87-8_geol_map_chehalisriver_westport_100k.zip]

Logan, R. L., 2003, Geologic map of the Shelton 1:100,000 quadrangle, Washington: Washington Division of Geology and Earth Resources Open File Report 2003-15, 1 sheet, scale 1:100,000. [http://www.dnr.wa.gov/publications/ger_ofr2003-15_geol_map_shelton_100k.pdf]

Logan, R. L.; Walsh, T. J., 2009, Mima Mounds formation and their implications for climate change [abstract]. In Northwest Scientific Association, The Pacific Northwest in a changing environment—Northwest Scientific Association 81st annual meeting; Program with abstracts: Northwest Scientific Association, p. 38-39. [http://www.northwestscience.org/Resources/Final%20Annual%20Meeting%20Abstracts%20and%20Programs/2009%20NWSA%20Program%20and%20Abstracts.pdf]

Logan, R. L.; Walsh, T. J., 2004, Geologic map of the Summit Lake 7.5-minute quadrangle, Thurston and Mason Counties, Washington: Washington Division of Geology and Earth Resources Open File Report 2004-10, 1 sheet, scale 1:24,000. [http://www.dnr.wa.gov/Publications/ger_ofr2004-10_geol_map_summitlake_24k.pdf]

Logan, R. L.; Walsh, T. J.; Stanton, B. W.; Sarikhan, I. Y., 2009, Geologic map of the Maytown 7.5-minute quadrangle, Thurston County, Washington: Washington Division of Geology and Earth Resources Geologic Map GM-72, 1 sheet, scale 1:24,000. [http://www.dnr.wa.gov/publications/ger_gm72_geol_map_maytown_24k.pdf]

Lowry, W. D.; Baldwin, E. M., 1952, Late Cenozoic geology of the lower Columbia River valley, Oregon and Washington: Geological Society of America Bulletin, v. 63, no. 1, p. 1-24, 1 plate.

Ludwig, K. R., 2003, User's manual for Isoplot 3.00—A geochronological toolkit for Microsoft Excel: Berkeley Geochronology Center, Special Publication No. 4a, 1 v.

Mallory, V. S., 1959, Lower Tertiary biostratigraphy of the California Coast Ranges: American Association of Petroleum Geologists, 416 p., 7 plates.

Marillo-Sialer, E.; Woodhead, J.; Hanchar, J. M.; Reddy, S. M.; Greig, A.; Hergt, J.; Kohn, B., 2016, An investigation of the laser-induced zircon 'matrix effect': Chemical Geology, v. 438, p. 11-24. [https://doi.org/10.1016/j.chemgeo.2016.05.014]

Martin, H.; Smithies, R. H.; Rapp, R.; Moyen, J. F.; Champion, D., 2005, An overview of adakite, tonalite–trondhjemite–granodiorite (TTG), and sanukitoid: relationships and some implications for crustal evolution: Lithos, v. 79, no. 1-2, p. 1-24. [https://doi.org/10.1016/j.lithos.2004.04.048]

McCaffrey, Robert; King, R. W.; Payne, S. J.; Lancaster, Matthew, 2013, Active tectonics of northwestern U.S. inferred from GPS-derived surface velocities: Journal of Geophysical Research Solid Earth, September, v. 118, 15 p. [http://onlinelibrary.wiley.com/doi/10.1029/2012JB009473/epdf]

McCaffrey, Robert; Qamar, A. I.; King, R. W.; Wells, Ray; Khazaradze, Giorgi; Williams, C. A.; Stevens, C. W.; Vollick, J. J.; Zwick, P. C., 2007, Fault locking, block rotation and crustal deformation in the Pacific Northwest: Geophysical Journal International, v. 169, no. 3, p. 1315-1340.

Min, K.; Mundil, R.; Renne, P. R.; Ludwig, K. R., 2000, A test for systematic errors in ^{40}Ar-^{39}Ar geochronology through comparison with U-Pb analysis of a 1.1 Ga rhyolite: Geochimica et Cosmochimica Acta, no. 64, p. 73-98.

Moothart, S. R., 1993, Geology of the middle and upper Eocene McIntosh Formation and adjacent volcanic and sedimentary rock units, Willapa Hills, Pacific County, southwest Washington: Oregon State University Master of Science thesis, 265 p., 3 plates. [http://ir.library.oregonstate.edu/xmlui/handle/1957/12293]

Morrison, R. B., 1991, Introduction. *In* Morrison, R. B., editor, Quaternary nonglacial geology—Conterminous U.S.: Geological Society of America DNAG Geology of North America, v. K-2, p. 1-12.

Newcomb, R. C., 1952, Origin of the Mima Mounds, Thurston County region, Washington: Journal of Geology, v. 60, no. 5, p. 461-472.

Noble, J. B.; Wallace, E. F., 1966, Geology and ground-water resources of Thurston County, Washington; Volume 2: Washington Division of Water Resources Water-Supply Bulletin 10, v. 2, 141 p., 5 plates. [https://fortress.wa.gov/ecy/publications/summarypages/wsb10b.html]

Parker, K. W.; Crider, J. G.; Poland, M. P., 2005, The Mount Baker volcano—Revisiting the 20-year-old trilateration network in Mount Baker wilderness, Washington [abstract]: Geological Society of America Abstracts with Programs, v. 37, no. 4, p. 48.

Parsons, T. E.; Wells, R. E.; Fisher, M. A.; Flueh, E. R.; ten Brink, U. S., 1999, Three-dimensional velocity structure of Siletzia and other accreted terranes in the Cascadia forearc of Washington: Journal of Geophysical Research, v. 104, no. B8, p. 18,015-18,039.

Pease, M. H., Jr.; Hoover, Linn, Jr., 1957, Geology of the Doty–Minot Peak area, Washington: U.S. Geological Survey Oil and Gas Investigations Map OM-188, 1 sheet, scale 1:62,500. [https://ngmdb.usgs.gov/Prodesc/proddesc_5340.htm]

Pettijohn, F. J., 1957, Sedimentary rocks: Harper and Brothers, 718 p.

Polenz, Michael; Alldritt, Katelin; Heheman, N. J.; Sarikhan, I. Y.; Logan, R. L., 2009, Geologic map of the Belfair 7.5-minute quadrangle, Mason, Kitsap, and Pierce Counties, Washington: Washington Division of Geology and Earth Resources Open File Report 2009-7, 1 sheet, scale 1:24,000. [http://www.dnr.wa.gov/Publications/ger_ofr2009-7_geol_map_belfair_24k.pdf]

Polenz, Michael; Allen, M. D.; Legorreta Paulín, Gabriel; Eungard, D. W.; Cakir, Recep; Scott, S. P.; Mahan, S. A., 2016, Geologic map of the Shelton Valley 7.5-minute quadrangle, Mason County, Washington: Washington Division of Geology and Earth Resources Map Series 2016-02, 1 sheet, scale 1:24,000, 45 p. text. [http://www.dnr.wa.gov/publications/ger_ms2016-02_geol_map_shelton_valley_24k.zip]

Polenz, Michael; Contreras, T. A.; Czajkowski, J. L.; Legorreta Paulín, Gabriel; Miller, B. A.; Martin, M. E.; Walsh, T. J.; Logan, R. L.; Carson, R. J.; Johnson, C. N.; Skov, R. H.; Mahan, S. A.; Cohan, C. R., 2010, Supplement to geologic maps of the Lilliwaup, Skokomish Valley, and Union 7.5-minute quadrangles, Mason County, Washington—Geologic setting and development around the Great Bend of Hood Canal: Washington Division of Geology and Earth Resources Open File Report 2010-5, 27 p. [http://www.dnr.wa.gov/publications/ger_ofr2010-5_lilliwaup_skokomish_valley_union_suppl_24k.pdf]

Polenz, Michael; Favia, J. G.; Hubert, I. J.; Legorreta Paulín, Gabriel; Cakir, Recep, 2015, Geologic map of the Port Ludlow and southern half of the Hansville 7.5-minute quadrangles, Kitsap and Jefferson Counties, Washington: Washington Division of Geology and Earth Resources Map Series 2015-02, 1 sheet, scale 1:24,000, 40 p. text. [http://www.dnr.wa.gov/publications/ger_ms2015-02_geol_map_port_ludlow_hansville_24k.zip]

Polenz, Michael; Gordon, H. O.; Hubert, I. J.; Contreras, T. A.; Patton, A. I.; Legorreta Paulín, Gabriel; Cakir, Recep, 2014, Geologic map of the Center 7.5-minute quadrangle, Jefferson County, Washington: Washington Division of Geology and Earth Resources Map Series 2014-02, 1 sheet, scale 1:24,000, with 35 p. text. [http://www.dnr.wa.gov/publications/ger_ms2014-02_geol_map_center_24k.zip]

Polenz, Michael; Petro, G. T.; Contreras, T. A.; Stone, K. A.; Legorreta Paulín, Gabriel; Cakir, Recep, 2013, Geologic map of the Seabeck and Poulsbo 7.5-minute quadrangles, Kitsap and Jefferson Counties, Washington: Washington Division of Geology and Earth Resources Map Series 2013-02, 1 sheet, scale 1:24,000, with 39 p. text. [http://www.dnr.wa.gov/publications/ger_ms2013-02_geol_map_seabeck-poulsbo_24k.zip]

Pratt, T. L.; Johnson, S. Y.; Potter, C. J.; Stephenson, W. J.; Finn, C. A., 1997, Seismic reflection images beneath Puget Sound, western Washington State—The Puget Lowland thrust sheet hypothesis: Journal of Geophysical Research, v. 102, no. B12, p. 27,469-27,489.

Prescott, J. R.; Hutton, J. T., 1994, Cosmic ray contribution to dose rates for luminescence and ESR dating—Large depths and long-term time variations: Radiation Measurements, v. 23, no. 2-3, p. 497-500.

Pringle, P. T.; Goldstein, B. S.; Anderson, N. R., 2000, Tanwax Creek–Ohop Valley late-glacial flood—Evidence that discharge from an ice-dammed lake in the Carbon River Valley was augmented by a temporary landslide dam, Puget Lowland, Washington [abstract]. *In* Washington Department of Ecology; Washington Hydrologic Society; U.S. Geological Survey, Program and abstracts from the Third Symposium on the Hydrogeology of Washington State: Washington Department of Ecology, p. 85.

Pringle, P. T.; Goldstein, B. S., 2002, Deposits, erosional features, and flow characteristics of the late-glacial Tanwax Creek–Ohop Creek Valley flood—A likely source for sediments composing the Mima Mounds, Puget Lowland, Washington [abstract]: Geological Society of America Abstracts with Programs, v. 34, no. 5, p. A-89.

Rau, W. W., 1958, Stratigraphy and foraminiferal zonation in some of the Tertiary rocks of southwestern Washington: U.S. Geological Survey Oil and Gas Investigations Chart OC-57, 2 sheets.

Rau, W. W., 1981, Pacific Northwest Tertiary benthonic foraminiferal biostratigraphic framework—An overview: Geological Society of America Special Paper 184, p. 67-84. [http://www.dnr.wa.gov/publications/ger_ofr80-5_foraminiferal_biostratigraphic_framework.pdf]

Rau, W. W., 2004, Pacific Northwest Tertiary foraminiferal collections of the U.S. Geological Survey and the State of Washington: Washington Division of Geology and Earth Resources Digital Report 4, 1 CD-ROM. [http://www.dnr.wa.gov/publications/ger_dr4_pacific_nw_foram_collections.zip]

Reed, S.; Amundson, R., 2012, Using LIDAR to model Mima mound evolution and regional energy balances in the Great Central Valley, California: Geological Society of America Special Papers, v. 490, p. 21-41.

Rigg, G. B., 1958, Peat resources of Washington: Washington Division of Mines and Geology Bulletin 44, 272 p. [http://www.dnr.wa.gov/publications/ger_b44_peat_reasources_wa_3.pdf]

Ritchie, A. M., 1953, The erosional origin of the Mima mounds of southwest Washington: Journal of Geology, v. 61, no. 1, p. 41-50.

Sarikhan, I. Y.; Stanton, K. D.; Contreras, T. A.; Polenz, Michael; Powell, Jack; Walsh, T. J.; Logan, R. L., 2008, Landslide reconnaissance following the storm event of December 1-3, 2007, in western Washington: Washington Division of Geology and Earth Resources Open File Report 2008-5, 16 p. [http://www.dnr.wa.gov/publications/ger_ofr2008-5_dec2007_landslides.pdf]

Sarikhan, Isabelle; Thompson, Elizabeth; Heinitz, Anne, 2009, Quick report—Landslide reconnaissance during the January 7, 2009, storm: Washington Division of Geology and Earth Resources Quick Report, January 7, 2009.

Schasse, H. W., compiler, 1987, Geologic map of the Centralia quadrangle, Washington: Washington Division of Geology and Earth Resources Open File Report 87-11, 28 p., 1 plate, scale 1:100,000. [http://www.dnr.wa.gov/publications/ger_ofr87-11_geol_map_centralia_100k.zip]

Schasse, H. W.; Logan, R. L.; Polenz, Michael; Walsh, T. J., 2003, Geologic map of the Shelton 7.5-minute quadrangle, Mason and Thurston Counties, Washington: Washington Division of Geology and Earth Resources Open File Report 2003-24, 1 sheet, scale 1:24,000. [http://www.dnr.wa.gov/Publications/ger_ofr2003-24_geol_map_shelton_24k.pdf]

Schmandt, Brandon; Humphreys, Eugene, 2011, Seismically imaged relict slab from the 55 Ma Siletzia accretion to the northwest United States: Geology, v. 39, no. 2, p. 175-178.

Siddall, M.; Rohling, E. J.; Thompson, W. G.; Waelbroeck, C., 2008, Marine isotope stage 3 sea level fluctuations—Data synthesis and new outlook: Reviews of Geophysics, v. 46, RG4003. [doi:10.1029/2007RG000226]

Simonetti, Antonio; Heaman, L. M.; Hartlaub, R. P.; Creaser, R. A.; MacHattiea, T. G.; Bohmb, Christian, 2005, U-Pb zircon dating by laser ablation-MC-ICP-MS using a new multiple ion counting Faraday collector array: Journal of Analytical Atomic Spectrometry, v. 20, no. 8, p. 677-686.

Singhroy, V. H.; Kenny, F. M.; Barnett, P. J., 1992a, Imagery for Quaternary geological mapping in glaciated terrains: Canadian Journal of Remote Sensing, v. 18, no. 2, p. 112-117.

Singhroy, V. H.; Kenny, F. M.; Barnett, P. J., 1992b, Quaternary mapping in glaciated and vegetated areas using SAR and multispectral images: Proceeding I, XVII International Society of Photogrammetry and Remote Sensing congress, Washington, D.C., v. XXIX, part B7. [http://www.isprs.org/proceedings/XXIX/congress/part7/874_XXIX-part7.pdf]

Snavely, P. D., Jr.; Brown, R. D., Jr.; Roberts, A. E.; Rau, W. W., 1958, Geology and coal resources of the Centralia–Chehalis district, Washington, with a section on the microscopical character of Centralia–Chehalis coal by J. M. Schopf: U.S. Geological Survey Bulletin 1053, 159 p., 6 plates.

Snavely, P. D., Jr.; Rau, W. W.; Hoover, Linn, Jr.; Roberts, A. E., 1951, McIntosh Formation, Centralia–Chehalis coal district, Washington: American Association of Petroleum Geologists Bulletin, v. 35, no. 5, p. 1052-1061.

Snavely, P. D., Jr.; Rau, W. W.; Hoover, Linn, Jr.; Roberts, A. E., 1959, McIntosh Formation, Centralia–Chehalis coal district, Washington. *In* Washington Division of Mines and Geology, Tertiary stratigraphic papers, southwestern Washington: Washington Division of Mines and Geology Reprint 3, 10 p. [http://www.dnr.wa.gov/publications/ger_reprint3_strat_papers_sw_wa.pdf]

Squires, R. L.; Goedert, J. L., 1994, New species of early Eocene small to minute mollusks from the Crescent Formation, Black Hills, southwestern Washington: Veliger, v. 37, no. 3, p. 253-266.

Tepper, J.; Clark, K.; Asmerom, Y.; McIntosh, W., 2002, Eocene adakites associated with initiation of Cascade subduction, Puget lowlands, WA [abstract]: Eos (American Geophysical Union Transactions), v. 83, no. 47, Supplement, p. F1466.

Thorson, R. M., 1980, Ice-sheet glaciation of the Puget Lowland, Washington, during the Vashon Stade (late Pleistocene): Quaternary Research, v. 13, no. 3, p. 303-321.

Trehu, A. M.; Asudeh, Isa; Brocher, T. M.; Luetgert, J. H.; Mooney, W. D.; Nabelek, J. L.; Nakamura, Y., 1994, Crustal architecture of the Cascadia forearc: Science, v. 266, no. 5183, p. 237-243.

Troost, K. G., 1999, The Olympia nonglacial interval in the southcentral Puget Lowland, Washington: University of Washington Master of Science thesis, 123 p. [https://fortress.wa.gov/dnr/geologydata/library/thesis/Troost1999_Olym_nonglacial.pdf]

Troost, K. G., 2016, Chronology, lithology and paleoenvironmental interpretations of the penultimate ice-sheet advance into the Puget Lowland, Washington State: University of Washington Doctor of Philosophy thesis, 239 p.

Troost, K. G.; Booth, D. B., 1999, The Seattle geologic mapping project—A new collaborative research project at the University of Washington. *In* Booth, D. B.; Troost, K. G.; Weaver, C. S.; Steele, W. K., Seattle urban geologic hazards workshop: University of Washington Department of Geological Sciences [and others], 6 p., unpaginated.

Troost, K. G.; Booth, D. B., 2008, Geology of Seattle and the Seattle area, Washington. *In* Baum, R. L.; Godt, J. W.; Highland, L. M., editors, Landslides and engineering geology of the Seattle, Washington, area: Geological Society of America Reviews in Engineering Geology XX, p. 1-35. [http://www.wou.edu/las/physci/taylor/g473/seismic_hazards/troost_booth_2008_geo_seattle.pdf]

U.S. Department of Agriculture, Natural Resource Conservation Service, Soil Survey Staff, 2013, Web soil survey, Mason County, Washington: U.S. Department of Agriculture. [accessed on 12/2013 and 7/2014 at http://websoilsurvey.nrcs.usda.gov/]

U.S. Geological Survey Geologic Names Committee, 2010, Divisions of geologic time—Major chronostratigraphic and geochronologic units: U.S. Geological Survey Fact Sheet 2010-3059, 2 p. [http://pubs.usgs.gov/fs/2010/3059/]

Walker, J. D.; Geissman, J. W., compilers, 2009, Geologic time scale: Geological Society of America, 1 p. [http://www.geosociety.org/science/timescale/timescl.pdf]

Walsh, T. J.; Korosec, M. A.; Phillips, W. M.; Logan, R. L.; Schasse, H. W., 1987, Geologic map of Washington—Southwest quadrant: Washington Division of Geology and Earth Resources Geologic Map GM-34, 2 sheets, scale 1:250,000, with 28 p. text. [http://www.dnr.wa.gov/publications/ger_gm34_geol_map_sw_wa_250k.pdf]

Walsh, T. J.; Logan, R. L., 2005, Geologic map of the East Olympia 7.5-minute quadrangle, Thurston County, Washington: Washington Division of Geology and Earth Resources Geologic Map GM-56, 1 sheet, scale 1:24,000. [http://www.dnr.wa.gov/publications/ger_gm56_geol_map_eastolympia_24k.pdf]

Wang, Kelin, 1996, Simplified analysis of horizontal stresses in a buttressed fore arc sliver at an oblique subduction zone: Geophysical Research Letters, v. 23, no. 16, p. 2021-2024.

Washburn, A. L., 1988, Mima mounds—An evaluation of proposed origins with special reference to the Puget Lowlands: Washington Division of Geology and Earth Resources Report of Investigations 29, 53 p. [http://www.dnr.wa.gov/publications/ger_ri29_mima_mounds.pdf]

Washington Geological Survey, 2016a, Landslides and landforms—GIS data, July, 2016: Washington Division of Geology and Earth Resources Digital Data Series 12, version 4.2, previously released February 2016. [http://www.dnr.wa.gov/publications/ger_portal_landslides_landforms.zip]

Washington Geological Survey, 2016b, Surface geology, 1:100,000—GIS data, November 2016: Washington Division of Geology and Earth Resources Digital Data Series DS-18, version 3.1, previously released June 2010. [http://www.dnr.wa.gov/publications/ger_portal_surface_geology_100k.zip]

Wells, R. E.; Blakely, R. J.; Wech, A. G.; McCrory, P. A.; Michael, Andrew, 2017, Cascadia subduction tremor muted by crustal faults: Geology, doi:10.1130/G38835.1.

Wells, R. E.; McCaffrey, Robert, 2013, Steady rotation of the Cascade arc: Geology, v. 41, no. 9, p. 1027-1030.

Wells, R. E.; Weaver, C. S.; Blakely, R. J., 1998, Cascadia forearc migration and its neotectonic significance [abstract]: Eos (American Geophysical Union Transactions), v. 79, no. 45, Supplement, p. F874.

Wells, Ray; Bukry, David; Friedman, Richard; Pyle, Doug; Duncan, Robert; Haeussler, Peter; Wooden, Joe, 2014, Geologic history of Siletzia, a large igneous province in the Oregon and Washington Coast Range—Correlation to the geomagnetic polarity time scale and implications for a long-lived Yellowstone hotspot: Geosphere, July 14th, 2014, 28 p. [Supplemental Information: http://geosphere.gsapubs.org/content/10/4/692/suppl/DC1]

Appendix A. New Radiocarbon Age Estimate

Table A1. Radiocarbon data from site GD1. ^{14}C yr BP age estimate is in radiocarbon years before 1950, and uncertainty estimates are reported at 1σ (68% confidence). Age in ka is in calendar years before 1950 divided by 1,000 and has 2σ uncertainty range. An age range is preferred because uncertainties are unequally distributed as a result of the calibration curves used to convert between radiocarbon and calendar years. Uncertainty statements reflect random and lab errors; errors from unrecognized sample characteristics or flawed methodological assumptions (for example, ^{14}C sample contamination from younger carbon flux) are not known. Age is adjusted for measured $^{13}C/^{12}C$ ratio (a 'conventional' age).

Geologic units are the interpretation of this study. Elevations were estimated using Puget Sound Lidar Consortium lidar data projected to State Plane South, NAD 83 HARN, U.S. Survey feet, supplemented by visual elevation estimates on-site. Lidar elevation statements were not adjusted to account for systematic projection differences relative to the base map. Lidar level '0' is theoretically 3.40 to 3.47 ft below base map level '0' [http://www.ngs.noaa.gov/cgi-bin/VERTCON/vert_con.prl]. Latitude and longitude coordinates are in WGS84.

^{14}C site ID (geologic unit)		Reference	Material	Method	$^{13}C/^{12}C$ (o/oo)	Age estimate
GD1 (Qoa)		this study	wood	^{14}C	-23.8	13,970 ±40 ^{14}C yr BP (17.075–16.850 ka)
Lab ID[a]	Beta-452498	Sample from 29 g of uncompressed, wood (gymnosperm or angiosperm; species unknown, possibly cedar) from a 5 cm (1.97 in.) thick stick extracted from otherwise apparently barren, seemingly massive, 5 ft thick exposure of olive-gray, soft clay. Stick was sampled 6 ft below the surface, about 1 ft below the top of the host clay, which was overlain by 1 ft of sandy pebble gravel (unit Qa?) that was in turn overlain by 4 ft of silt (unit Qa from active flood plain). The entire section was exposed along an active eastern channel-wall cutbank of Waddell Creek. The stick lacked bark and thickened away from the exposed face as we dug into the exposure. It was embedded to >50 cm (>19.7 in.) depth, at which point we broke it off to sample the outer portion. It remains unclear if the stick is detrital or part of a snag drowned in place.				
TRS	sec. 29, T17N R3W					
Lat/long. (degrees)	46.93695 -123.07917					
Elev. (ft)	303					

[a] Beta Analytic.

Appendix B. New Luminescence Age Estimates

Table B1. Infrared-stimulated luminescence (IRSL) and optically stimulated luminescence (OSL) results from age site GD2. Analyses were performed on fine-grained feldspar (IRSL) and quartz (OSL) by Shannon Mahan and Harrison Gray, USGS. Ages and errors are rounded, and uncertainty estimates are 1σ (68% confidence), as reported by the lab. Uncertainty statements reflect random and lab errors; errors from unrecognized sample characteristics or flawed methodological assumptions (for example, incomplete pre-depositional resetting of luminescence samples) are not known.

Luminescence site ID (geologic unit)	Water content (%)[a]	K (%)[b]	U (ppm)[b]	Th (ppm)[b]	Cosmic dose additions (Gy/ka)[c]	Equivalent dose (Gy)	Total dose rate (Gy/ka)	N[e]	Scatter (%)[e]	Method	Age (ka)
GD2 (Qpo)	14 (32)	0.86 ±0.04	0.66 ±0.12	2.64 ±0.28	0.18–0.12	116 ±4.05[d]	1.58 ±0.10[d]	14 (15)	42	IRSL	65.820 ±4.590[d]
						70.1 ±1.80[e]	1.19 ±0.07[f]	16 (18)	43	OSL	58.910 ±3.960[f]

Lab ID	Lrj065b
TRS	sec. 34, T17N R3W
Lat/long. (degrees)	46.91364 -123.05093
Elev. (ft)	220
Material	sand

Sand, compact, well sorted, stained red, sampled from a private driveway roadcut east of Waddell Creek Road just south of bridge across Waddell Creek. Sample is part of a 10 ft thick package of pale orange, medium- to fine-grained, well-sorted, rounded to subangular, compact sand with moderate iron staining and some secondary clay. Deposit is bedded and crossbedded and includes sparse lenses of pebbles. Down-section continuation of exposure farther southeast reveals that the sample was collected close to the upper end of at least 25 ft of stream-channel section with interbeds and lenses of cobbly pebble gravel in the lower 15 ft (Schematic Section 1). Analyses (OSL and IRSL) suggest MIS 4–age (71–57 ka, Lisiecki and Raymo, 2005). Lab notes that if this is a glacial deposit, then it is unsurprising that the infrared-stimulated luminescence date from feldspar is older than the optically stimulated luminescence date from quartz. Assuming the dates are accurate, the deposit is either distal proglacial outwash, or reworked from older proglacial outwash (see *Weathering*).

[a] Field moisture, with number in parentheses indicating the complete sample saturation percent. Ages calculated using approximately 50 percent of saturation values.

[b] Analyses obtained using high-resolution gamma spectrometry (HPGe detector).

[c] Cosmic doses and attenuation with depth were calculated using the methods of Prescott and Hutton (1994).

[d] Dose rate and age for fine-grained 250–180 microns K-feldspar, post IR230C; fade of 3.4%/decade. Exponential + linear fit used on equivalent dose.

[e] Number of replicated equivalent dose (De) estimates used to calculate the equivalent dose. Number in parentheses indicates total number of measurements included in calculating the represented equivalent dose and age using the minimum age model (MAM).

[f] Dose rate and age for fine-grained 250–180 micron-sized quartz. Exponential + linear fit used on single aliquot regeneration equivalent doses.

Appendix C. New $^{40}Ar/^{39}Ar$ Age Estimate

Table C1. $^{40}Ar/^{39}Ar$ age for site GD3 (Fig. M1). Analysis by Daniel Miggins and staff, Argon Geochronology Lab, College of Earth, Ocean, and Atmospheric Sciences, Oregon State University, Corvallis, Oregon. Uncertainty values span 2σ (95% confidence). Uncertainty statements reflect random and lab errors; errors from unrecognized sample characteristics or flawed methodological assumptions (for example, unrecognized post-depositional re-setting of $^{40}Ar/^{39}Ar$ ratios) are not known. – – – indicates no data.

$^{40}Ar/^{39}Ar$ site (sample ID) (geologic unit)			Plagioclase from surficial exposure of dark gray, fine-grained (aphanitic) basalt (geochemistry site G8) that forms a hill (inselberg) above the surrounding outwash gravel terrace. The hill and basalt exposures extend into the Littlerock quadrangle, but the sample for geochemistry and age control was collected 330 ft east of the Littlerock quadrangle in the adjacent Maytown quadrangle, where fresher rock was accessible due to driveway blasting. Thin-section petrographic analysis showed 55–60% euhedral and porphyritic subhedral plagioclase with 20–25% anhedral clinopyroxene, 15% clay alteration, and 5% opaque minerals. The texture is trachytic, interstitial, and porphyritic. 49.53 ±0.26 Ma date from whole-rock groundmass dismissed due to ^{39}Ar recoil. Complete analytical results from both groundmass and plagioclase are provided in data supplement.					
GD3 (Lrj002) (Evb)							
TRS	sec. 36, T17N R3W						
Lat/long (degrees)	46.92279 -123.00024						
Elev. (ft)	220						
Result Type	**$^{40}Ar^{(r)}/^{39}Ar^{(k)}$**	**±2σ**	**$^{39}Ar^{(k)}$ (%.n)**	**K/Ca ±2σ**	**Age (Ma) ±2σ**		**MSWD**
Age Plateau	16.12097	±0.0706	93.46	0.0030 ±0.0001	45.97	±0.23	0.60
		±0.44%	37			±0.50%	97%
					Full external error	±1.06	
					Analytical error	±0.20	
Total Fusion	16.04492	±0.07637	40	0.0031 ±0.000	45.75	±0.24	
		±0.48%	– – –			±0.53%	

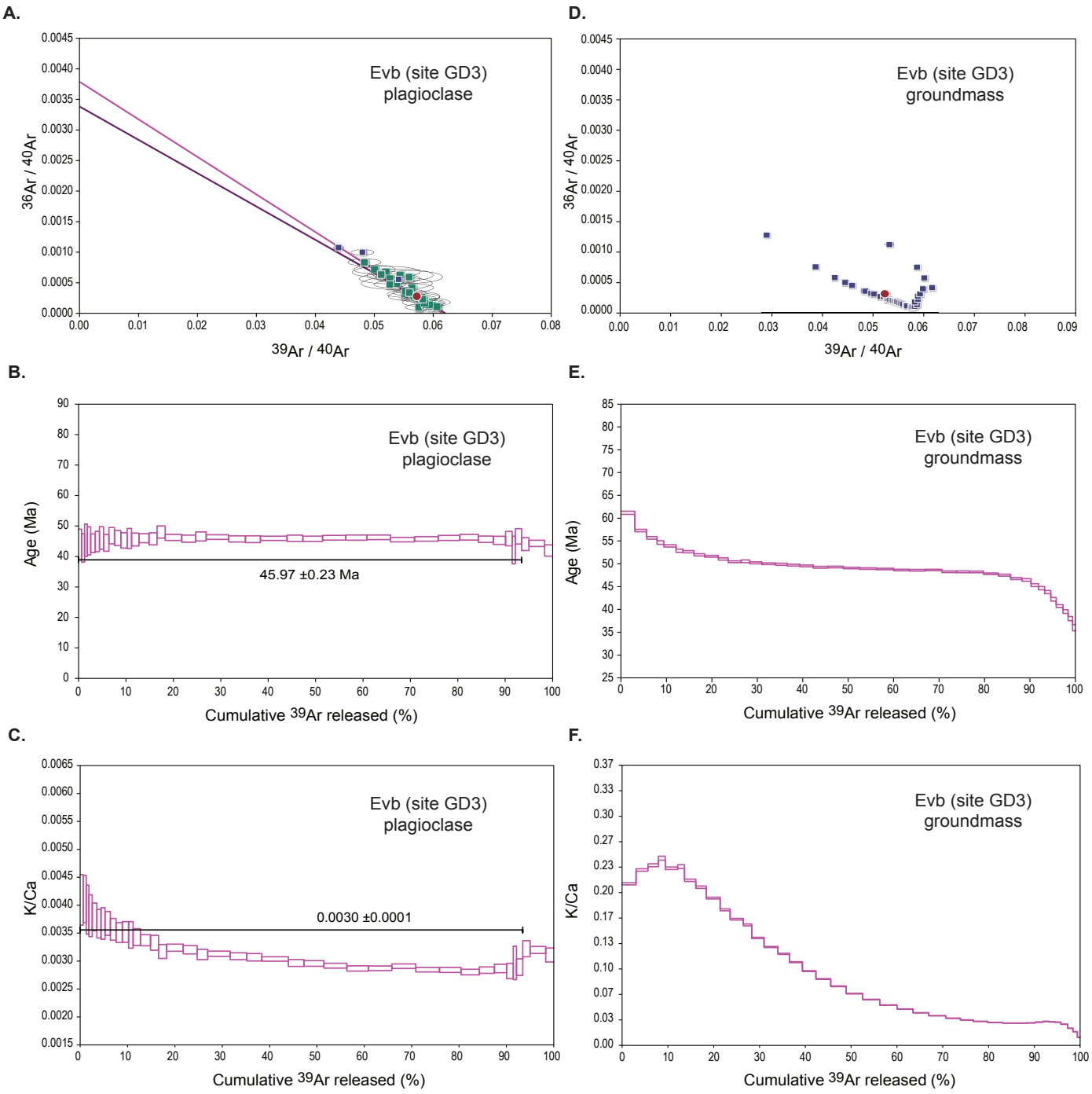

Figure C1. Step-heating results for $^{40}Ar/^{39}Ar$ analysis on plagioclase (Figs. A, B, and C) and groundmass (Figs. D, E, and F) of basalt from unit Evb at age site GD3. Figures A and D are concordia diagrams. Due to an internally consistent signal pattern in the plagioclase analysis compared to a signal pattern that suggests a partly open system in the groundmass analysis, the lab favors the plagioclase analysis. Figures B and E present step-heating results with a well-defined age plateau in the plagioclase analysis (Fig. B). Black bars in Figs. B and C identify heating steps included in age estimate. Figs. C and F show the step-heating evolution of the K/Ca ratio.

Appendix D. New U-Pb Age Estimate

U-PB ANALYSIS METHODS

Each sample (~5 kg) was crushed to fine sand-sized particles. Heavy minerals were then concentrated using a Wilfley table. Between each sample great care was taken to clean crushing plates and the Wilfley table to reduce the risk of contamination. The zircon concentrate was then passed through a 220-µm sieve and the <220-µm fraction was sorted by magnetic separation using a Frantz LB1 to remove undesirable magnetic minerals. Zircons were then separated by density from the non-magnetic fraction using di-methylene iodide heavy liquid. From the zircon separate, ~50–100 individual zircon grains were hand selected from each sample and mounted in epoxy. The grain mount was polished to expose the grain centers and regions suitable for analysis were identified from Cathodoluminescense imaging.

U-Pb zircon data were collected at the Canadian Center for Isotopic Micro-analysis (CCIM) at the University of Alberta using procedures modified from Simonetti and others (2005). The analytical setup consists of a New Wave UP-213 laser ablation system interfaced with a Nu plasma MC-ICPMS equipped with three ion counters for static collection of Pb isotopes. We operated the laser at 4 Hz pulse rate with a beam diameter of 30 µm at a fluence of ~3 J/cm^2. Ablations were conducted in a He atmosphere at a flow rate of 1 L/min through the cell. Output from the cell was joined to the output from a standard Nu plasma desolvating nebulizer (DSN-100). On peak gas + acid blanks (30s) were measured prior to a set of 10–20 analyses. Data were collected statically, consisting of 30 1-second integrations. Before and after each set of analyses, we analyzed zircon reference materials, GJ-1 (Jackson and others, 2004; Heaman, unpublished data), and 94–35 (Klepeis and others, 1998) to monitor U-Pb fractionation, reproducibility, and instrument drift. Mass bias for Pb isotopes was corrected by simultaneously measuring $^{205}Tl/^{203}Tl$ from an aspirated 0.5 ppb Tl solution (NIST SRM 997) using an exponential mass fractionation law and assuming a natural $^{205}Tl/^{203}Tl$ of 2.3871.

All data were reduced offline using an Excel©-based spreadsheet. Unknowns were normalized to the zircon reference material GJ-1 and the uncertainties reported are a quadratic combination of: (1) the standard error of the measured isotope ratio (internal precision) and (2) the standard deviation of the standard means (external precision). The external precision of the GJ1 zircon reference material is estimated to be ~1% at 2σ for $^{207}Pb/^{206}Pb$ and 2%, 2σ for $^{206}Pb/^{238}U$ during these analytical sessions. The secondary standard 94-35 treated as an unknown yielded a lower Tera-Wasserberg concordia intercept age of 55.61 ±0.39 Ma (2σ, MSWD, 0.65, n = 18), in excellent agreement with the 55.5 Ma ID-TIMS age of Klepeis and others (1998). Data points were discarded if it was obvious that an inclusion contributed to analysis, there was an extreme common Pb component, or the grain was in fact not zircon. All plots were generated using the Isoplot software of Ludwig (2003).

Table D1. U-Pb data from age site GD4. Analysis by S. Andrew DuFrane and staff at ICPMS Lab, Canadian Center for Isotopic Micro-analysis, Department of Earth & Atmospheric Sciences, University of Alberta, Edmonton, Alberta, Canada T6G 2E3. Uncertainty values are at the 2σ level, but due to the large number analyses, the intercept age error is unrealistically low for this technique and reflects random errors only. Systematic errors from unrecognized sample characteristics are not well understood, but likely amount to ~2% (Marillo-Sialer and others, 2016, and references therein). Thus a more realistic estimate of the total uncertainty for the intercept age is ~2%, (1 Ma).

U-Pb site ID (sample ID) (geologic unit)		Age estimate	MSWD
GD4 (Lrm340b2) (Em2m)		47.35 ±0.21 Ma	1.08
TRS	sec. 8, T16N R3W	Date marks formation of 50 zircon grains sampled from a tuffaceous sandstone bed in thin- to medium-bedded marine claystone to siltstone. See *Data Supplement* for analytical results and age estimates from individual crystals. Thin-section petrographic analysis shows plagioclase as only major mineral; minor minerals include pyroxene, hornblende, actinolite, biotite, opaque mineral grains, quartz, lithics (basalt, maybe an andesite, some polycrystalline quartz, and mica cement), and other minerals. Most grains are subangular to subrounded, monocrystalline, and anhedral. Many of the feldspars are zoned and twinned and appear to be a fragment of a larger crystal, because they contain only a portion of what was apparently concentric zoning in a larger crystal. What initially appears as evenly fine-grained matrix mostly consists of ghost clasts vaguely outlined by more birefringent material (mica?). The ghost clasts appear well rounded and similar in size to the feldspar clasts. A few clasts are altered (to clay?) basalt grains that contain many very small, lathe-shaped crystals (mostly altered) at random orientations. Some lithic clasts contain larger plagioclase pieces, and a few are polycrystalline quartz(?), some with jagged margins between the crystals.	
Lat/long. (degrees)	46.88037 -123.08307		
Elev. (ft)	260		

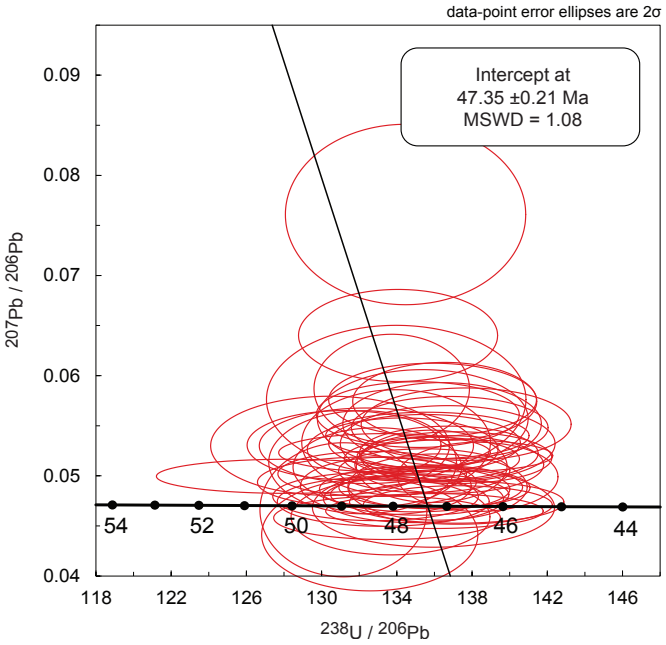

Figure D1. Semi-Total Lead Isochron (Tera-Wasserburg) Diagram of $^{207}Pb/^{206}Pb$ vs. $^{238}U/^{206}Pb$ ratios for 50 zircon analyses from age site GD4. The approximately horizontal line across the lower diagram is the concordia curve (along which the $^{207}Pb/^{206}Pb$ age equals the $^{238}U/^{206}Pb$ age). Black dots on the curve mark concordant ages (54 to 44 Ma). The intercept of the regression line (steep, thin black line) with the concordia curve provides an age estimate at 47.35 Ma and assumes a closed system with neither gain nor loss of non-radiogenic uranium or lead. The MSWD (mean square of weighted deviates) near 1 indicates that the computed uncertainty adequately covers the range of individual ages.